PHILOSOPHICAL TRANSACTIONS A

royalsocietypublishing.org/rsta

CC BY

Research

Cite this article: Kerr GH *et al*. 2026 Tropospheric Ozone Assessment Report II: Changing health impacts of global ozone exposure. *Phil. Trans. R. Soc. A* **384**: 20250268.
https://doi.org/10.1098/rsta.2025.0268

Received: 31 December 2025
Accepted: 1 June 2026

One contribution of 8 to a theme issue 'Tropospheric Ozone Assessment Report II'.

Subject Areas:
atmospheric science, atmospheric chemistry, climatology, meteorology, environmental engineering

Keywords:
atmospheric composition, tropospheric ozone, respiratory health, health impacts, air quality, climate change

Author for correspondence:
Gaige H. Kerr
e-mail: gaigekerr@gwu.edu

†These are lead authors, as denoted by Tropospheric Ozone Assessment Report II.

Supplementary material is available online at https://doi.org/10.6084/m9.figshare.c.8654423.

THE ROYAL SOCIETY PUBLISHING

Tropospheric Ozone Assessment Report II: Changing health impacts of global ozone exposure

Gaige H. Kerr[1], Kofi Amegah[2,†], Lulu Chen[1,†], James L. Crooks[3,4,†], Drew Shindell[5,†], Dimitris Akritidis[6,7], Karn Vohra[8], Susan C. Anenberg[1], Christopher Carlsten[9], Forrest Lacey[10], Soo-Yeon Kim[1], Jintai Lin[11], M. Omar Nawaz[12], Pallavi Pant[13], Andrea Pozzer[7,14], Louis Rivoire[15], Erika von Schneidemesser[16], Martin G. Schultz[17,18], Steven T. Turnock[19], Shuxiao Wang[20,21], J. Jason West[22] and Yingying Yan[23]

[1]Department of Environmental and Occupational Health, George Washington University, Washington, DC, USA
[2]Department of Biomedical Sciences, University of Cape Coast, Accra, Ghana
[3]Division of Biostatistics and Bioinformatics, National Jewish Health, Denver, CO, USA
[4]Department of Epidemiology, Colorado School of Public Health, Aurora, CO, USA
[5]Nicholas School of the Environment, Duke University, Durham, NC, USA
[6]Department of Meteorology and Climatology, School of Geology, Aristotle University of Thessaloniki, Thessaloniki, Greece
[7]Atmospheric Chemistry Department, Max-Planck-Institut für Chemie, Mainz, Germany
[8]School of Geography, Earth and Environmental Sciences, University of Birmingham, Birmingham, UK
[9]Division of Respiratory Medicine, Faculty of Medicine, The University of British Columbia, Vancouver, British Columbia, Canada
[10]National Center for Atmospheric Research, Boulder, CO, USA

© 2026 The Authors. Published by the Royal Society under the terms of the Creative Commons Attribution License http://creativecommons.org/licenses/by/4.0/, which permits unrestricted use, provided the original author and source are credited.

Downloaded from royalsocietypublishing.org/rsta/article-pdf/doi/10.1098/rsta.2025.0268/6174166/rsta.2025.0268.pdf
by guest
on 09 November 2026

[11]Laboratory for Climate and Ocean-Atmosphere Studies,
Department of Atmospheric and Oceanic Sciences, School of Physics,
Peking University, Beijing, People's Republic of China
[12]School of Earth and Environmental Sciences, Cardiff University, Cardiff, UK
[13]Health Effects Institute, Boston, MA, USA
[14]Climate and Atmospheric Research Center, The Cyprus Institute, Nicosia, Cyprus
[15]Department of Earth, Atmospheric, and Planetary Sciences, Massachusetts Institute of Technology, Cambridge, MA, USA
[16]Research Institute for Sustainability, Potsdam, Germany
[17]Jülich Supercomputing Centre, Forschungszentrum Jülich Institute for Advanced Simulation, Julich, Germany
[18]Department of Mathematics and Computer Science, University of Cologne, Cologne, Germany
[19]Hadley Centre, Met Office, Exeter, UK
[20]State Key Laboratory of Regional Environment and Sustainability, School of Environment, Tsinghua University, Beijing, People's Republic of China
[21]Key Laboratory of Sources and Control of Air Pollution Complex, Ministry of Ecology and Environment of the People's Republic of China, Beijing, People's Republic of China
[22]Department of Environmental Sciences and Engineering, Gillings School of Global Public Health, The University of North Carolina at Chapel Hill, Chapel Hill, NC, USA
[23]Department of Atmospheric Science, School of Environmental Sciences, China University of Geosciences, Wuhan, People's Republic of China

GHK, 0000-0001-8869-0752; KA, 0000-0001-5868-6402; LC, 0000-0002-8929-3414; JLC, 0000-0002-0021-5701; DS, 0000-0003-1552-4715; DA, 0000-0003-3104-5271; KV, 0000-0001-6570-0663; SCA, 0000-0002-9668-603X; CC, 0000-0003-2455-6575; FL, 0000-0003-4578-8375; S-YK, 0000-0002-4959-0879; JL, 0000-0002-2362-2940; MON, 0000-0001-7706-7287; PP, 0000-0003-0251-6580; AP, 0000-0003-2440-6104; LR, 0000-0002-3030-7922; EVS, 0000-0003-1386-285X; MGS, 0000-0003-3455-774X; STT, 0000-0002-0036-4627; JJW, 0000-0001-5652-4987; YY, 0009-0006-2270-0229

As part of the second Tropospheric Ozone Assessment Report (TOAR-II), we synthesize global observations and observationally constrained estimates of surface-level ozone (O_3) with contemporary literature to characterize the global distribution and trends of long-term O_3 exposure, focusing on two health-relevant metrics and health impacts attributable to long-term exposure. The highest 2016–2020 surface-level O_3 concentrations are observed or estimated in South Asia, eastern China, and parts of the Middle East and North Africa. From 2000 to 2020, O_3 declined across southeastern North America and parts of Eastern Europe, while the largest increases occurred in South Asia and Sub-Saharan Africa. Global premature mortality from chronic obstructive pulmonary disease (COPD) attributable to long-term O_3 exposure nearly doubled between 2000 and 2020, reaching approximately 500 000 deaths annually. This overall increase obscures decreasing attributable deaths across North America and Europe and increasing deaths across large parts of the Global South. To spur high-quality, robust research on O_3 health impacts, we summarize state-of-the-science practices for conducting health impact assessments (HIAs) and characterizing associated uncertainty. We also call for expanded *in situ* monitoring, improved health datasets and epidemiologic evidence, and sustained precursor emission reductions to clarify and limit the growing global health burden of O_3 under climate change and demographic shifts.

This article is part of the theme issue 'Tropospheric Ozone Assessment Report II'.

Downloaded from royalsocietypublishing.org/rsta/article-pdf/doi/10.1098/rsta.2025.0268/6174166/rsta.2025.0268.pdf
by guest
on 09 November 2026

1. Introduction

The nexus of ozone (O_3) and human health has a storied history. Following its formal identification in 1839 by Christian Schönbein, O_3 was lauded as a panacea, evidenced by an 1873 book suggesting O_3 'be pumped into […] cities, and be dosed through fever wards, sick rooms, the crowded localities of the poor' [1,2]. However, during the postwar economic boom of the late 1940s and 1950s, industrialized areas such as Los Angeles faced increasingly common and severe O_3 episodes [3,4], and related health research raised concerns that O_3 posed a detriment—not a benefit—to human health [5,6]. It is worth noting that these early studies were largely qualitative in nature. Rather than isolating O_3 as the putative agent driving health impacts, they generally referred to the broader concept of 'smog' [7]. Additionally, health outcomes primarily focused on acute symptoms, specifically irritation of the eyes, skin and respiratory tract.

Since this time, researchers have deepened our knowledge of the biological mechanisms underlying O_3-attributable health effects, and epidemiologic studies have demonstrated their population-level impacts (e.g. [8]). Increased awareness of these impacts has spurred the development, promulgation and enforcement of health-protective standards, and about half of all countries had ambient O_3 standards by the late 2010s [9,10]. Ozone's impacts on populations distant from emission sources have also led to international coordination through the United Nations Economic Commission for Europe (UNECE) Convention on Long-Range Transboundary Air Pollution (CLRTAP), which convened the Task Force on Hemispheric Transport of Air Pollution (TF-HTAP). These and related activities have advanced our understanding of transboundary O_3 pollution [11–13] and—by showing that coordinated O_3 precursor species reductions can decrease O_3 in North America and Europe—have informed policy (e.g. Gothenburg Protocol revisions) [14].

Prior to around 2000, health studies and the United States Environmental Protection Agency (EPA) National Ambient Air Quality Standards largely relied on daily 1-hour maximum concentrations. This metric, however, failed to capture adverse effects from lower but sustained O_3 exposure [15]. Subsequent evidence demonstrated health impacts from prolonged 6–8-hour exposure [16], leading researchers and policymakers to adopt 8-hour average metrics. Two are now widely used: the daily maximum 8-hour average (DMA8) O_3 and the 6-month ozone season average DMA8 (OSDMA8) O_3. Regulatory agencies within China, India, Korea, the United States and the European Union base their standards on DMA8 O_3, and the World Health Organization (WHO) has recommended DMA8 O_3 targets and guidelines [17]. The WHO also has recommendations for OSDMA8 O_3, and this metric is used by Global Burden of Disease (GBD) studies.

Understanding O_3-attributable health impacts requires accurate and geographically representative measurements or estimates of ambient O_3 concentrations, which serve as proxies for exposure and are used in epidemiologic studies, as true individual-level exposure is not directly observable and ambient concentrations provide the best available estimate of population-average conditions. The financial, material and human resources required for *in situ* monitoring have largely limited such monitoring to wealthier nations. Even when resources are available, harmonizing regional or national datasets presents additional hurdles. The Tropospheric Ozone Assessment Report (TOAR) partially addresses these challenges by creating a unified database of observed O_3 concentrations, precursors and meteorological data, which allows users to produce customized statistics and trends. During the first phase of TOAR (TOAR-I), the health assessment—hereafter referred to as *TOAR-I Health* [10]—explored the distribution of 2010–2014 surface-level O_3 and longer-term trends from 2000 to 2014 using five different O_3 metrics relevant to acute and chronic exposure. These metrics included:

— the fourth highest DMA8 concentration in a year, which is a regulated quantity by the United States EPA;
— the number of days per year with DMA8 concentrations greater than 70 parts-per-billion by volume (ppbv);

Downloaded from royalsocietypublishing.org/rsta/article-pdf/doi/10.1098/rsta.2025.0268/6174166/rsta.2025.0268.pdf
by guest
on 09 November 2026

— the annual sum of daily DMA8 concentrations over 35 ppbv, which is an exposure indicator considered by the European Environment Agency;
— the annual maximum of the 3-month running mean of daily maximum 1-hour concentrations, which was the exposure metric in the GBD Study 2010 and 2013 but is not currently used; and
— OSDMA8 concentrations, representing the locally defined 6-month period of peak O_3 concentrations each year (further described in §4).

TOAR-I Health found the highest O_3 concentrations in western North America, southern Europe and East Asia. Trends were generally consistent across metrics, but the magnitude and significance depended on whether the metric emphasized peak season versus seasonal or annual concentrations. Peak metrics were more likely to show significant increasing trends in East Asia and significant decreasing trends in North America and Europe, whereas annual or seasonal averages often produced weaker or non-significant trends. In addition, while *TOAR-I Health* examined health-relevant trends, there was little discussion of the estimated burden of disease attributable to O_3 exposure.

Here, in TOAR's second phase (TOAR-II), we update and expand upon *TOAR-I Health* in several ways. Although many geoscientists are aware of adverse health effects from O_3 exposure, far fewer understand the underlying pathophysiology and epidemiology. To address this gap, we synthesize evidence on the causal pathways connecting O_3 exposure to disease, drawing on insights from both mechanistic and epidemiologic studies (§§2 and 3). We leverage the updated TOAR-II database and observationally constrained, high-resolution gridded estimates of surface-level O_3 to map the recent (2016–2020) spatial distribution of and 2000–2020 trends in long-term O_3 exposure (see §4 and §§5 and 6). Of the five metrics considered in *TOAR-I Health*, this assessment considers two—annual average DMA8 and OSDMA8—reflecting their continued use in epidemiologic research and environmental health; the remaining metrics are either regulatory indicators not widely used in environmental health or have been superseded in the GBD Study by alternative exposure metrics. We then place estimates of O_3-attributable disease burdens, primarily from the GBD Study 2021, in the context of these updated exposure fields to evaluate how spatial patterns and trends in O_3 relate to the global distribution of health impacts (§7). Finally, we discuss best practices for conducting health impact assessments (HIAs) and characterizing associated uncertainties (§8) and analyse how future emissions, climate change, demographics and population-level health may alter O_3 exposure and health impacts (§9).

2. Pathophysiology of ozone-related health effects

The primary mechanisms underlying the pathogenesis of O_3-attributable disease are summarized by the exposure-induced response portion of figure 1. Upon inhalation, O_3 dissolves in the epithelial lining fluid covering the pulmonary alveoli, where gas exchange and blood oxygenation occur. The low water solubility of O_3 allows it to reach the lower respiratory tract, where it triggers the formation of secondary oxidants [18,19]. The oxidative stress induced by these secondary species can lead to cellular injury and an inflammatory response, typically neutrophilic, that affects blood oxygenation [19]. The five steps comprising the exposure-induced response in figure 1 may not always occur or occur in order; as examples, inflammation can be triggered without step 3 or step 4, and clinically important effects may occur without substantial inflammation.

The disease pyramid in figure 1 illustrates how cellular damage manifests both sub-clinically, as biological changes not yet producing symptoms, and clinically, as observable disease or measurable symptoms. The tissue injury, airway inflammation and increased airway resistance are key responses to O_3 exposure and produce characteristic sequelae measurable as lung function reductions on pulmonary function tests [18,20–23]. Together, these processes illustrate how exposure initiates injury and inflammation that can impair pulmonary function and contribute to clinical outcomes quantified in epidemiologic studies.

Downloaded from royalsocietypublishing.org/rsta/article-pdf/doi/10.1098/rsta.2025.0268/6174166/rsta.2025.0268.pdf
by guest
on 09 November 2026

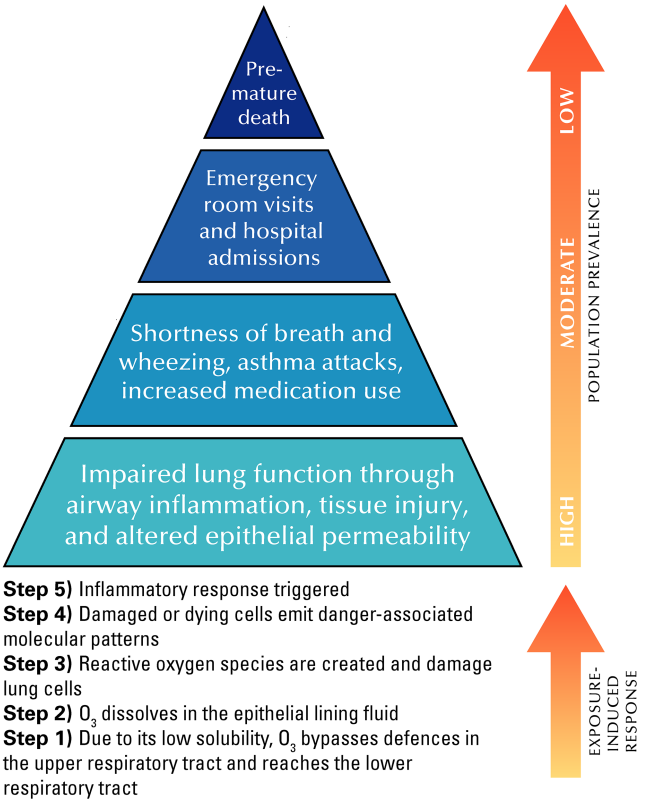


Figure 1. The exposure-induced response at the bottom summarizes how O_3 exposure contributes to the pathogenesis of attributable disease by triggering immune responses or altering host physiology. The epidemiologic pyramid model illustrates sub-clinical impacts of O_3 exposure at the bottom leading to clinical effects at the top, and the width of each layer is qualitatively proportional to the number of individuals affected. Pyramid position reflects prevalence, not intrinsic severity.

3. Ozone epidemiology and health evidence

Landmark air pollution epidemiology studies of the 1980s and 1990s focused specifically on O_3 exposure and set the stage for over 30 years of research on population-level health impacts. These studies linked exposure to reduced lung function and asthma onset and severity, leveraging regional cohorts (e.g. California's Seventh-day Adventists, Harvard Six Cities) [24,25] and nationwide cohorts (e.g. National Health and Nutrition Examination Survey) [26]. The historically deepest evidence linking exposure with adverse health outcomes is for short-term (often 1-, 8-, or 24-hour) exposure [27]. Short-term exposure is causally linked to respiratory morbidity [18,19,27–30]. Multi-city analyses in North America also report increased respiratory mortality from short-term exposure and suggest a link with cardiovascular mortality [31–33], though that link is less supported [27]. Other studies have reported increased risk of all-cause mortality in response to elevated short-term exposure in cities in Asia [34], North America and Europe [35], and worldwide [36] and also suggest a causal relationship between short-term exposure and central nervous system effects [27,37]. The strength and plausibility of O_3 as a causal agent for acute endpoints are increased substantially by controlled human exposure studies, where potential confounding is virtually eliminated (e.g. [38]).

Our assessment primarily focuses on long-term O_3 exposure and associated health impacts. Effect estimates linking long-term exposure to mortality for select studies, notable for their large cohorts, long follow-up and rigorous exposure assessment, are listed in table 1. Large-scale US studies demonstrate an association between long-term O_3 exposure and elevated risks of

Downloaded from royalsocietypublishing.org/rsta/article-pdf/doi/10.1098/rsta.2025.0268/6174166/rsta.2025.0268.pdf
by guest
on 09 November 2026

Downloaded from royalsocietypublishing.org/rsta/article-pdf/doi/10.1098/rsta.2025.0268/6174166/rsta.2025.0268.pdf
by guest
on 09 November 2026

Table 1. Summary of epidemiologic effect estimates for mortality outcomes from long-term O_3 exposure in select large-scale cohort studies. Effect estimates are reported as relative risks (RRs) or hazard ratios (HRs), as provided in the original studies. A tilde (∼) next to the lowest measured concentration signifies that the concentration was not explicitly provided in studies but instead inferred from figures.

cohort; location	population	impact	lowest measured concentration	effect estimate (per 10 ppbv)	notes	reference
American Cancer Society Cancer Prevention Study-II (ACS CPS-II); United States (US)	≥30 yrs ($n = 448\,850$)	respiratory	33.3 ppbv (6-month average of daily maximum)	1.04 (95% CI 1.01–1.07)	cardiovascular mortality only showed increased HR in one pollutant model	[39]
ACS CPS-II; US	≥30 yrs ($n = 669\,046$)	respiratory cardiovascular (circulatory plus diabetes) all-cause	26.7 ppbv (annual DMA8)	1.12 (1.08–1.16) 1.03 (1.01–1.05) 1.02 (1.01–1.04)	study draws on the same ACS CPS-II cohort as Jerrett *et al.* [39] but with additional participants	[40]
National Institutes of Health-American Association of Retired Persons Diet and Health Study; US	≥50 yrs ($n = 548\,780$)	respiratory cardiovascular	26.8 ppbv (annual DMA8)	1.04 (1.00–1.09) 1.03 (1.01–1.06)	also examined associations using 6-month average DMA8, which changed effect estimates marginally while associations remained significant	[41]
Canadian Census Health and Environment Cohort; Canada	≥25 yrs and <90 yrs ($n = 2\,448\,500$)	respiratory cardiovascular	∼20 ppb (6-month average DMA8)	1.04 (1.01–1.07)[a] 1.16 (1.14–1.18)[a]	results from one-pollutant models, but study also examined other models	[42]
China Chronic Disease and Risk Factor Surveillance; China	≥18 yrs ($n = 96\,955$)	cardiovascular	∼28 ppbv (6-month average DMA8)	1.18 (1.10–1.27)		[43]
Chinese Electric health Records Research in Yinzhou (CHERRY) Study; Yinzhou, Zhejiang Province, China	≥18 yrs ($n = 744\,882$)	cardiovascular	30.5 ppb (annual average of daily average)	1.22 (1.12–1.33)		[44]

(*Continued.*)

Downloaded from royalsocietypublishing.org/rsta/article-pdf/doi/10.1098/rsta.2025.0268/6174166/rsta.2025.0268.pdf
by guest
on 09 November 2026

Table 1. (*Continued.*)

cohort; location	population	impact	lowest measured concentration	effect estimate (per 10 ppbv)	notes	reference
Demographic and Health Surveys Program; low-income and middle-income countries	<5 yrs ($n = 1\,244\,409$)	all-cause	~25 ppbv (6-month average DMA8)	1.06 (1.02–1.11)		[45]
Global Burden of Disease (GBD) Study 2021; meta-analysis of cohort studies from Canada, the United Kingdom, and the US	N/A	COPD	uniform distribution around the minimum and fifth percentile of summer season concentrations from Turner *et al.*, [40], i.e. ~U(29.1, 35.7 ppbv)	1.074 (1.014–1.137)	used a Bayesian, regularized, trimmed (MR-BRT) meta-regression tool to estimate relative risk	[46]

[a]*RR values converted from the original unit of per 10.503 ppb change in* O_3.

respiratory and cardiovascular mortality [39–41]. Notably, cohort studies from China and Canada have found even stronger associations between ozone exposure and cardiovascular mortality than US studies [42,43,47]. Many of these epidemiologic studies focused on the entire adult population (table 1), but associations between exposure and adverse health outcomes exist across age strata. Recent research highlights significant childhood health effects in the United States and low- and middle-income countries [21,45] and effects in older populations in Canada and China [48,49]. Although table 1 summarizes effect estimates for O_3-attributable mortality, long-term O_3 exposure has been linked to impaired lung function and incident asthma in children; asthma-related emergency visits, hospitalizations and symptoms; development of chronic obstructive pulmonary disease (COPD) and allied conditions; higher hospitalization rates for respiratory diseases; and reproductive and cardiovascular effects [23,27,50–53]. Multiple studies also suggest neurodegenerative effects from long-term exposure [54–56] and, recently, long-term exposure has been linked to COVID-19 severity [57].

Recent United States EPA Integrated Science Assessments (ISAs) conclude that the strongest evidence for long-term O_3 exposure is for respiratory outcomes, which they judge as 'likely […] a causal relationship' in their weight-of-evidence assessment [27,58]. The ISAs also evaluate total mortality, characterizing the evidence as 'suggestive of […] a causal relationship'. The WHO reviewed the literature on O_3 health effects when updating their air quality guideline (AQG) levels in 2021 [17] and deemed the long-term O_3-outcome associations as probably causal for respiratory effects and suggestive of being causal for total mortality, considering EPA and Health Canada findings [59]. The GBD applies a different evidence-grading framework (i.e. burden of proof risk function) [60], and Brauer *et al.* [46]—hereafter referred to as the GBD Study 2021—only included COPD mortality attributable to long-term exposure. This risk-outcome pair was classified as having 'weak evidence of association', receiving two stars on their five-star evidence-grading scale, similar to their designation for the association between second-hand smoke and tracheal, bronchus and lung cancer.

Other assessments note that health impacts of long-term O_3 exposure beyond the respiratory system remain less certain; for example, cardiovascular and cognitive effects and all-cause mortality were classified as 'suggestive of a causal relationship' [27]. Less confidence in the causality of associations could stem, in part, from including studies from Europe showing weak to no association or even protective effects of O_3 exposure [61,62]. Some of these studies, particularly from Europe, assess a narrower exposure range (approx. 36–48 ppbv) compared to the broader ranges observed in the US (approx. 24–61 ppbv) and Chinese (approx. 27–63 ppbv) studies. However, inconsistent findings may also reflect differences in how studies account for respiratory disease seasonality and co-pollutant and temperature confounding, which directly affect health and modulate O_3 formation. When co-pollutants are included in multi-pollutant models, the apparent protective associations with O_3 can weaken and move towards the null [63].

4. Material and methods

The TOAR-II database contains station-based O_3 observations at hourly or finer temporal resolution from 18 large air quality networks and many individual data providers [64]. Ozone-related air pollutant concentration data have been collected, harmonized in terms of formatting and metadata, and enhanced through an extensive set of metadata elements summarizing essential elements of a station's pollution signature [65] as well as through the extraction of point-based time series of meteorological reanalysis data.

Compared with the TOAR-I database, the TOAR-II database contains a vastly increased amount of processed data and increased customizability, through which end users can request aggregated and standardized metrics that follow TOAR-II statistical recommendations [66]. One aspect of these recommendations is a minimum of 75% temporal coverage within the aggregation interval at a given station to accept a datum as valid. Rudimentary quality control

Downloaded from royalsocietypublishing.org/rsta/article-pdf/doi/10.1098/rsta.2025.0268/6174166/rsta.2025.0268.pdf
by guest
on 09 November 2026

and some visual inspection are performed on data before ingestion into the TOAR-II database, but overall, the data quality control is less stringent than in the TOAR-I database because of the greater data volume. As TOAR-I showed, most data from quality-controlled monitoring networks exhibited few inconsistencies, but there are countries or regions where measurement accuracy is less well constrained.

We obtained station-based annual average DMA8 (= avgdma8epax in TOAR-II database) and OSDMA8 (= osdma8) O_3 for 2000–2020. These metrics are provided as mole fractions, but we refer to them as 'concentrations' in units of ppbv following common usage in environmental epidemiology and because nmol mol^{-1} and ppbv are effectively equivalent [67,68]. Annual average DMA8 represents the mean of daily maximum 8-hour average O_3 concentrations. Each daily maximum is the highest of the 17 overlapping 8-hour windows from 700 to 2300 hours local time. OSDMA8 is calculated as the maximum of the 6-month running monthly average DMA8, including January to March of the following year [69,70]. This wrapping around the calendar year addresses different seasonal cycles in boreal versus austral environments. Although OSDMA8 values are assigned to individual years, the metric is not strictly annual because of the 6-month averaging window and year overlap.

With yearly values for these two metrics, we further calculated two statistics. The first, median concentrations from 2016 to 2020, allows us to understand the recent spatial distribution of surface-level O_3 while reducing the influence of interannual variability, and this statistic was only calculated for stations with 3 or more years (or peak seasons, when using the OSDMA8 metric) of observations. The other statistic is trends in concentrations calculated for 2000–2020 to characterize long-term changes in O_3. For a given station, trends are reported only if at least 75% of all years provide observations that pass TOAR-II quality control criteria. Trends were calculated using median quantile regression, and two-tailed p-values from this model were used to assess the degree of statistical confidence we place in them, where statistical 'very high certainty' corresponds to $p \leq 0.01$, 'high certainty' to $0.01 < p \leq 0.05$, 'medium certainty' to $0.05 < p \leq 0.10$, 'low certainty' to $0.10 < p \leq 0.33$ and 'very low certainty or no evidence' to $p > 0.33$ [66]. These p-values are based on default standard errors, which assume independent and identically distributed residuals, and evaluate the null hypothesis of no trend. A two-tailed test is used because we do not assume the direction of trends *a priori*. This approach follows guidance for TOAR-II and is preferred to alternative approaches (e.g. generalized least squares, Sen–Theil estimator) as the median estimate is robust to small sample sizes and outliers; however, autocorrelation or heteroskedasticity in O_3 time series could affect the reliability of p-values, representing a limitation of this approach. Providing confidence ranges follows policy-relevant literature and Intergovernmental Panel on Climate Change guidelines to discuss uncertainty [66,71]. Throughout the assessment, we also present station data aggregated to a $2° \times 2°$ grid by calculating 2016–2020 median concentrations or 2000–2020 trends across all stations within each grid cell. We refer to this product as 'gridded observations'. This gridding reduces station overlap on global maps and clarifies large-scale spatial patterns that can be otherwise obscured by closely spaced stations with differing local influences. Within each grid cell, stations are equally weighted, so clusters of monitors may disproportionately influence grid-cell values.

The TOAR-II database classifies monitors as 'government', 'research', 'university' or 'non-profit', with the latter referring to data sourced from OpenAQ (https://openaq.org/). Because OpenAQ data often originate from real-time transmissions and are generally not validated and non-profit monitors only account for approximately 3% of all monitors in the database, we excluded them from our analysis. The database also classifies station environments (i.e. urban, rural, suburban, unknown) with a machine learning-based classification approach incorporating ancillary datasets such as population density, NO_x emissions, and nighttime light [72]. Because the ancillary datasets used in this approach characterize conditions in the mid-2010s, the assigned urbanicity represents each station's environment at that time. This static representation is a limitation, as land-use around monitors can change.

Downloaded from royalsocietypublishing.org/rsta/article-pdf/doi/10.1098/rsta.2025.0268/6174166/rsta.2025.0268.pdf
by guest
on 09 November 2026

The unbalanced sparse distribution of *in situ* monitors leaves much of the world without coverage and limits a holistic understanding of health-relevant O_3 variability and trends. Consequently, most recent health assessments rely on a geophysical-hybrid combination of *in situ* monitors, chemical transport modelling and satellite retrievals, hereafter referred to as 'data fusion products' (e.g. [73–77]). Accordingly, we augment observations from the TOAR-II database with gap-filled estimates of surface-level O_3 from a data fusion product [69]. This dataset employs the M^3Fusion technique to remove biases from modelled O_3 from nine global atmospheric models, Bayesian maximum entropy (BME) methods to align simulated O_3 with *in situ* observations (including those in the TOAR-II database), and high-resolution downscaling using a chemical transport model to improve spatial detail. The resulting product provides annual OSDMA8 O_3 concentrations from 1990 to 2017 and corresponding space-time variance, which reflects model uncertainty given the correlation structure and available *in situ* O_3 observations, at a spatial resolution of 0.1° × 0.1° (approx. 10 × 10 km). In the BME framework, *in situ* observations are treated as hard data with zero variance, yielding the lowest estimation uncertainty in regions with dense monitoring. Uncertainty increases with distance in space-time from observations; in data-sparse regions, the BME estimate reverts towards the multi-model composite, and its variance approaches that of the underlying model ensemble, reflecting the absence of observational constraints [69].

To support estimation of O_3-attributable disease burdens through 2020, the GBD extended this dataset by extrapolating 2018–2020 concentrations using a log–linear model based on the preceding decade (2008–2017). We downloaded the resulting merged time series (2000–2020) from the GBD Study 2021 and refer to it hereafter as the 'BME dataset'. As with *in situ* observations, we calculated 2016–2020 median OSDMA8 O_3 concentrations from the BME dataset to characterize the recent spatial patterns of surface-level O_3. The GBD did not assess the performance of the 2018–2020 extrapolated data against observations, and we note that this extrapolation does not capture the full interannual variability of O_3; it was designed to represent longer-term concentration trends relevant for chronic exposure assessment. By incorporating the extrapolated years into our 5-year median, we reduce the influence of year-to-year variability and retain a robust estimate of central O_3 concentrations. The BME dataset's annual space-time variance was summed in quadrature to obtain a multi-year aggregated variance, and we converted this aggregated variance ($ppbv^2$) to standard deviation (ppbv) for ease of interpretation. We also calculated trends and their statistical significance from this BME dataset using the aforementioned quantile regression approach [66].

When presenting regional concentrations or calculating regional trends, we weight concentrations by population counts to represent population exposure. Global population count estimates are from WorldPop, which provides annual 1 × 1 km counts (all ages) for 2000–2020 [78]. We regrid these counts to the 0.1° × 0.1° resolution of the BME dataset and calculate population-weighted O_3 concentrations for seven world regions as

$$O_{3,\ \text{population-weighted}} = \frac{\sum_i (O_3 \times \text{pop}_i)}{\sum_i \text{pop}_i}, \tag{4.1}$$

where pop refers to the population, and i indexes 0.1° × 0.1° grid cells within a given region. Regions follow the seven GBD super-regions and their 21 constituent regions (figure 5). Six of the super-regions are geographically contiguous, while the seventh region aggregates high-income countries in the Americas, Europe and Australasia.

From the GBD Study 2021, we obtained estimates of annual, country-level COPD mortality attributable to long-term O_3 exposure and associated metrics related to its contribution to the global burden of disease from all risk factors considered. GBD estimates of attributable mortality are compared with other studies identified through a scoping review of the literature. We searched Google Scholar, Web of Science and PubMed (last search date 5 June 2025) using combinations of the terms 'ozone' or 'O_3', 'mortality' or 'deaths' and 'global'. We filtered results to only global studies to ensure consistency in geographic coverage and to avoid introducing additional assumptions to reconcile sub-global estimates across differing spatial domains; those with estimates in years

Downloaded from royalsocietypublishing.org/rsta/article-pdf/doi/10.1098/rsta.2025.0268/6174166/rsta.2025.0268.pdf
by guest
on 09 November 2026

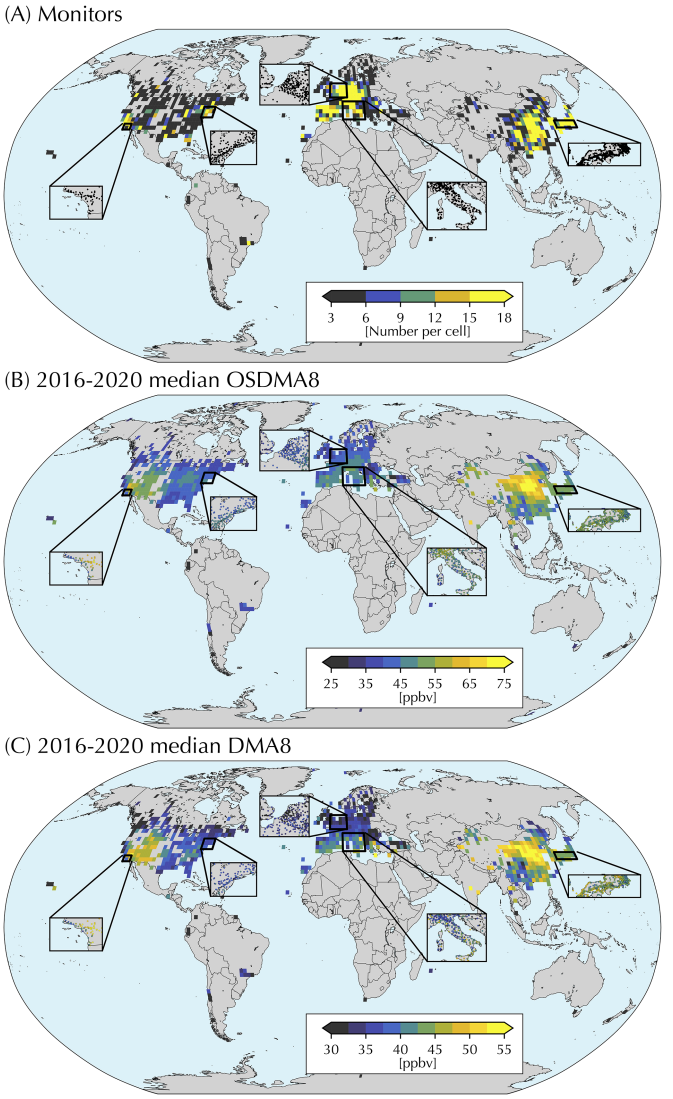


Figure 2. Density of *in situ* surface-level O_3 monitors and spatial variations in observed O_3 concentrations. (A) Monitor count in each 2° × 2° grid cell and, for the inset maps, the location of individual monitors. Median 2016–2020 (B) ozone season daily maximum 8-hour mixing ratio (OSDMA8) O_3 concentrations and (C) annual average daily maximum 8-hour mixing ratio (DMA8) O_3 concentrations. Grid-cell level shading in (B) and (C) is the median concentration over all monitors within each 2° × 2° grid cell, and coloured dots in inset maps depict monitor-level concentrations in some of the world's largest megalopolises that have a high density of monitors; larger maps of these monitor-level results are provided in supplementary material, figs. S2 and S3. Monitors in (A–C) are those included in the TOAR-II database following our inclusion criteria.

not within our long-term (2000–2020) trend period; and those that examined acute, rather than chronic, exposure effects on mortality.

5. Recent spatial distribution of surface-level ozone

Globally, 6335 unique monitors in the TOAR-II database provide sufficient data to be included in our analysis of the recent spatial distribution of surface-level O_3 (figure 2A and supplementary material, fig. S1), representing a 32.3% increase over the 4790 monitors included in *TOAR-I Health*,

Downloaded from royalsocietypublishing.org/rsta/article-pdf/doi/10.1098/rsta.2025.0268/6174166/rsta.2025.0268.pdf
by guest
on 09 November 2026

which used the same monitor inclusion criteria as ours (3 or more years within a 5-year period, 2010–2014). Nearly half (48.6%) of monitors are in TOAR-defined urban areas, with an almost even split between suburban (19.5%) and rural (18.3%) sites; 13.7% are classified as unknown.

Only 59 of 225 (26.2%) countries or territories have *in situ* monitors included in the TOAR-II database, with most (67.6%) located in the GBD-defined high income super-region (figure 2A and supplementary material, fig. S1). A majority of the 2020 global population (38.6% or 3.0 billion) lived in countries not represented in the database, many with limited or no publicly reported monitoring. These gaps are concentrated in the South Asia and Sub-Saharan Africa super-regions, which have only three and two monitors, respectively, that meet database and study inclusion criteria. Despite a global increase in the number of monitors since *TOAR-I Health*, some regions lost monitors that meet inclusion criteria (supplementary material, S1). For example, *TOAR-I Health* considered observations from 20 monitors in Sub-Saharan Africa, mostly from South Africa. The already minimal coverage declined to only two monitors in South Africa and Cape Verde for this assessment (supplementary material, fig. S1). Although figure 2 and supplementary material, fig. S1, broadly reflect the global distribution of monitors, more exist than we show. For example, observations from Iran [79] and Morocco [80] are discussed in the literature. Observations from India have increased in recent years, but persistent data quality issues [81] limit their robust use in this assessment.

We observe the lowest recent gridded concentrations (50 or less ppbv for OSDMA8 and 35 or less ppbv for median annual DMA8) throughout monitored portions of the northern United States, southern Canada and northern Europe (figure 2B,C). The highest gridded observations (70 or more ppbv for OSDMA8 and 50 or more ppbv for annual average DMA8) occurred across most of eastern China and in geographically limited parts of the southwestern United States and the Po Valley. Outside densely monitored regions, the few areas with limited observations (e.g. Brazil, Chile, South Africa, Cape Verde, etc.) generally have low concentrations. Observations in these under monitored regions are predominantly in urban areas, which might experience lower concentrations due to NOX titration.

At the station level (figure 2; supplementary material, figs. S2 and S3), the lowest OSDMA8 and annual average DMA8 concentrations were observed in urban areas of Bulgaria, Colombia, Canada, Great Britain and Türkiye, consistent with potential NO_x titration. The minimum across both metrics was at a station in İstanbul (2016–2020 median OSDMA8 = 14.5 ppbv; annual DMA8 = 11.9 ppbv). Low values were also found at rural stations in New Zealand and Argentina, probably reflecting limited precursors. By contrast, the highest concentrations occurred in China, with the maximum in Linfen, Shanxi Province (OSDMA8 = 82.5 ppbv; annual DMA8 = 61.8 ppbv). The mean tropospheric O_3 lifetime (10–40 days) [82–85] enables regional transport and supports the grid-cell aggregation of station-based concentrations (figure 2), though this can obscure local variability and may not hold in environments with shorter lifetimes (e.g. photochemically active boundary layers, coastal regions). For example, in southern California, coastal stations measure much lower concentrations than those approximately 10 km inland.

For our main analysis, we required stations to have 3 or more years of O_3 season data during 2016–2020. As a sensitivity, we relaxed this to a single year of data, which increased station counts by 15.9% (6335 to 7343; supplementary material, fig. S4). The high-income super-region showed one of the smallest relative increases (14.8%), indicating even coverage from year to year. By contrast, undermonitored super-regions such as North Africa, the Middle East, Latin America and the Caribbean experienced the largest increases (97.1% and 54.7%, respectively), suggesting more monitors exist but often with substantial missing data and/or insufficiently long time series (supplementary material, S1). At the grid-cell level, however, the spatial distribution of O_3 remains robust to inclusion criteria (cf. figure 2 and supplementary material, fig. S5).

Given the substantial gaps in *in situ* coverage, researchers have used models and data fusion methods to estimate global distributions of surface-level O_3. These efforts have included geostatistical methods (e.g. BME dataset) [69,86] and two machine learning studies [87,88] that estimate monthly average DMA8 O_3. Recent work has compared these three global ozone datasets as well

Downloaded from royalsocietypublishing.org/rsta/article-pdf/doi/10.1098/rsta.2025.0268/6174166/rsta.2025.0268.pdf
by guest
on 09 November 2026

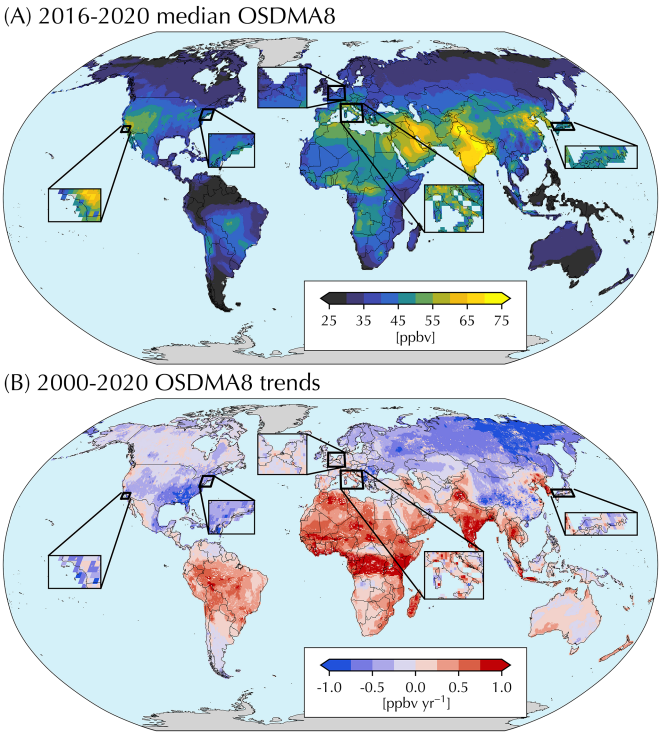


Figure 3. Spatial variations and trends in estimated O_3 concentrations using the Bayesian maximum entropy (BME) dataset. (A) 2016–2020 median OSDMA8 O_3 concentrations. (B) 2000–2020 median quantile regression trends in OSDMA8 O_3. The BME dataset does not estimate O_3 outside approximately −56°S to 75°N, and land masses outside these latitudes are shaded in grey.

as three chemical reanalysis studies with one another and with observations. This intercomparison reveals strikingly large disagreement among these datasets, with differences in average ozone of greater than 5 ppbv as well as differences in O_3 spatial distributions and long-term trends, despite the fact that these datasets are generated using some of the same input data [70]. This suggests that important uncertainties remain in our understanding of surface-level O_3 distributions globally. The rest of this section considers gap-filled estimates of 2016–2020 median OSDMA8 O_3 concentrations from the BME dataset [69], acknowledging that results would differ if we had chosen another concentration dataset. The global population-weighted concentration over this recent period was 48.1 ppbv, which is 1.6 times higher than the 2021 WHO AQG of approximately 30.6 ppbv (60 µg m^{-3}; [17]). The highest overall BME-estimated OSDMA8 O_3 concentrations (70 or more ppbv) are in South and East Asia and small pockets of the Middle East (figure 3A). These regions harbour many developing countries with rapidly increasing O_3 precursors [89,90]. However, it is worth noting that the extremely high BME-estimated OSDMA8 O_3 concentrations in India are not corroborated by systematically lower observations from ground-based monitors [81,91], which are typically roadside and may be influenced by NO_x titration. Most of South America and Australia have concentrations lower than 35 ppbv, but exceptions include higher concentrations in southeastern Brazil (e.g. the São Paulo-Rio de Janeiro urban corridor); remote northern Chile, where exceptional surface irradiance and clear skies accelerate photochemistry and frequent stratospheric-tropospheric exchanges occur [92,93]; and central-west Brazil, which experiences biomass-burning-driven production during the summer [94]. Estimated concentrations exceed 50 ppbv in the coastal northern and western parts of Africa, the latter of which is also influenced by biomass burning [95,96] and heatwaves [97]. Parts of Africa outside these regions generally have OSDMA8 O_3 concentrations under 50 ppbv. BME-estimated O_3 exhibits excellent agreement with

Downloaded from royalsocietypublishing.org/rsta/article-pdf/doi/10.1098/rsta.2025.0268/6174166/rsta.2025.0268.pdf
by guest
on 09 November 2026

observations by construction (cf. figures 2C and 3B), resulting in minimal uncertainty in monitored regions (supplementary material, fig. S6A). This agreement was also characterized by DeLang *et al.* [69], who compared the BME dataset against observations and found that it explained 81% of the variability with a root mean square error of 3.99 ppbv. Outside monitored regions, the uncertainty grows to approximately 15.2 ppbv, corresponding to the offset-removed observations, and reflects the loss of observational influence and reliance on the multi-model composite.

6. Long-term trends in surface-level ozone

We find pronounced long-term 2000–2020 decreases in gridded OSDMA8 O_3 concentrations in southeastern North America (less than −0.5 ppbv yr^{-1}), small increases throughout much of Western Europe and Japan (approx. 0–0.1 ppbv yr^{-1}), and larger increases in Korea (more than 0.5 ppbv yr^{-1}; figure 4A). The spatial distribution of annual average DMA8 O_3 trends (figure 4B) is broadly similar to OSDMA8 but with larger regions showing decreases in OSDMA8, rather than annual average DMA8 O_3. For instance, a larger portion of southeastern United States exhibits steeper declines in gridded OSDMA8 O_3 than in annual average DMA8 O_3, indicating that changes occur preferentially in certain seasons, with larger relative decreases during peak O_3 season but smaller or absent declines in annual averages.

At the station-level, about half (48.3%) of global monitors measure increasing trends in OSDMA8 O_3 and about two-thirds (64.9%) in annual average DMA8 O_3 (figure 4C,D; supplementary material, figs. S7 and S8). However, only 8.1% of monitor-level trends have high to very high certainty for OSDMA8 O3 and 18.0% for DMA8. Among urban stations, 74.1% show increasing OSDMA8 O_3 and 82.7% show increasing annual average DMA8 O_3, whereas most rural stations experience decreases (75.4% for OSDMA8 and 60.4% for annual average DMA8 O_3). This urban–rural contrast may reflect broader patterns of urbanization and industrialization, including migration from rural to urban areas and the associated increase in O_3 precursor emissions. For both metrics, a smaller proportion of stations show increasing O_3 trends at higher altitudes. For example, for annual average DMA8, 74.9% of stations below 125 m experience increases compared with 64.7% at 125–250 m, 52.2% at 250–500 m and 48.4% above 500 m. We did not detect a strong relationship between O_3 trends and latitude, though it should be noted that the range of trends in the northern mid-latitudes is much larger than that in other latitude bands.

Estimates from the BME dataset suggest that, in addition to southeastern North America, much of Eastern Europe and Central Asia showed long-term decreases between −0.25 and −0.75 ppbv yr^{-1} with very high or high certainty (figure 3B and supplementary material, fig. S6B). Canada and some parts of Oceania additionally exhibited weak decreases between 0 and −0.25 ppbv yr^{-1}, though with lower statistical certainty. By contrast, many regions with limited monitor coverage in Sub-Saharan Africa, South Asia and Latin America experienced increasing OSDMA8 O_3 with trends generally exceeding 0.5 ppbv yr^{-1} at very high or high certainty. The greatest increases, ranging between 1 and 2 ppbv yr^{-1}, are located on India's east coast as well as in an east-west Sub-Saharan corridor spanning the African continent from the Atlantic to the Indian Ocean.

Population-weighted global OSDMA8 O_3 concentrations increased at a rate of 0.19 ppbv yr^{-1} between 2000 and 2020, with high certainty. Population-weighted concentrations rose in 14 of 21 GBD-designated regions (figure 5). Trends in five of these regions exhibited either very high or high certainty. Increasing trends are largest in eastern and central Sub-Saharan Africa (0.67 and 0.54 ppbv yr^{-1}, respectively). Certainty in decreasing O_3 concentrations in the remaining third of GBD regions is overall high. The largest decreasing trends are in Eastern Europe and the high-income North America region (−0.42 and −0.33 ppbv yr^{-1}, respectively). The time series in figure 5 also illustrates different levels of interannual variability among regions. For example, the North Africa and Middle East region persistently experiences OSDMA8 O_3 concentrations around

Downloaded from royalsocietypublishing.org/rsta/article-pdf/doi/10.1098/rsta.2025.0268/6174166/rsta.2025.0268.pdf
by guest
on 09 November 2026

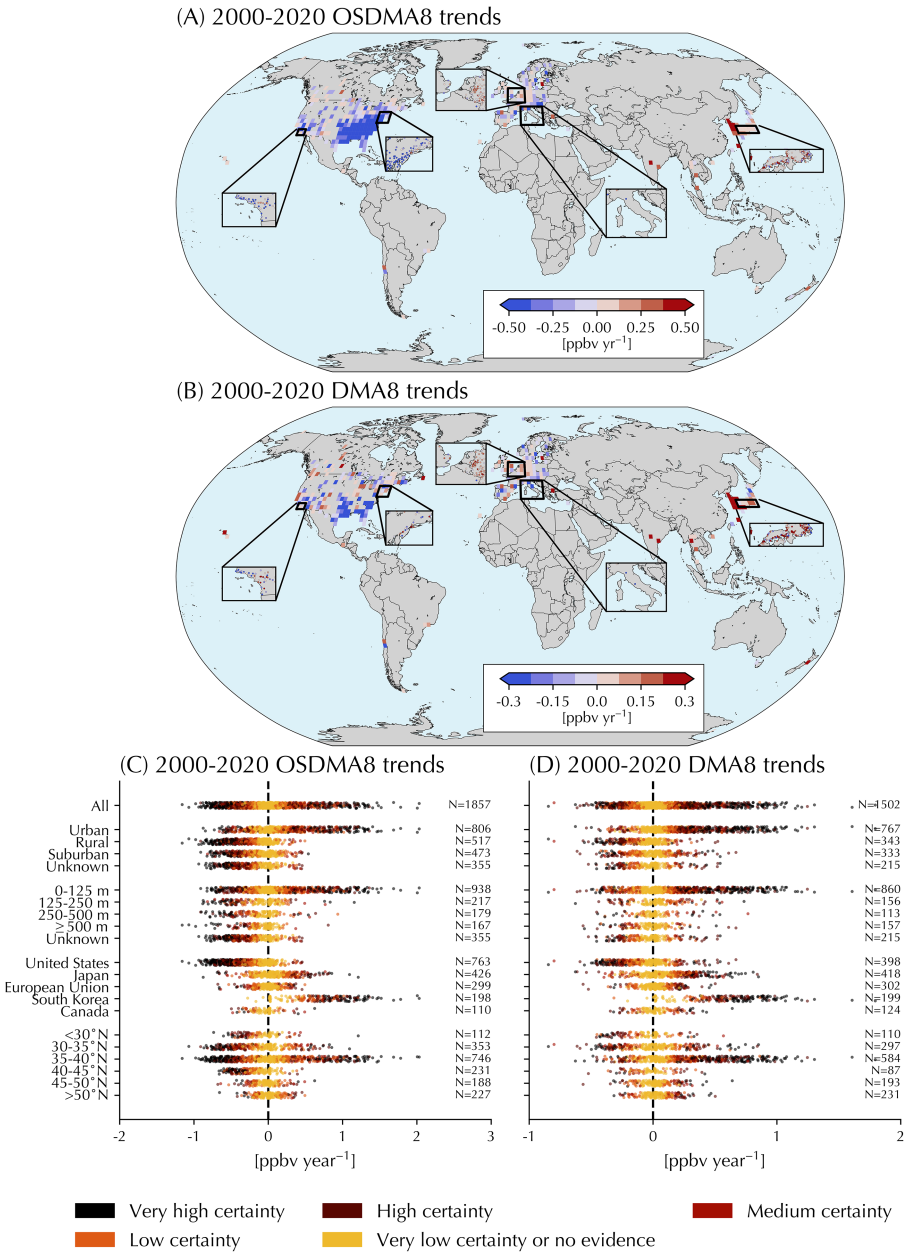


Figure 4. Observed O_3 trends. 2000–2020 median quantile regression trends in (A) OSDMA8 O_3 concentrations and (B) annual average DMA8 O_3 concentrations. Shading in (A) and (B) shows the median trend over all monitors within each 2° × 2° grid cell, and coloured dots in inset maps show monitor-level trends. Larger maps of these monitor-level trends are provided in supplementary material, figs. S7 and S8. The magnitude and significance of monitor-level trends in (C) OSDMA8 O_3 concentrations and (D) annual average DMA8, further categorized by environment (i.e. urban, rural, suburban), elevation, the five countries with the largest number of monitors and latitude. The sample size for each category is shown to the right of each distribution. Colours in (C) and (D) indicate the statistical significance of trends based on TOAR-II categories (see §4).

Downloaded from royalsocietypublishing.org/rsta/article-pdf/doi/10.1098/rsta.2025.0268/6174166/rsta.2025.0268.pdf
by guest
on 09 November 2026

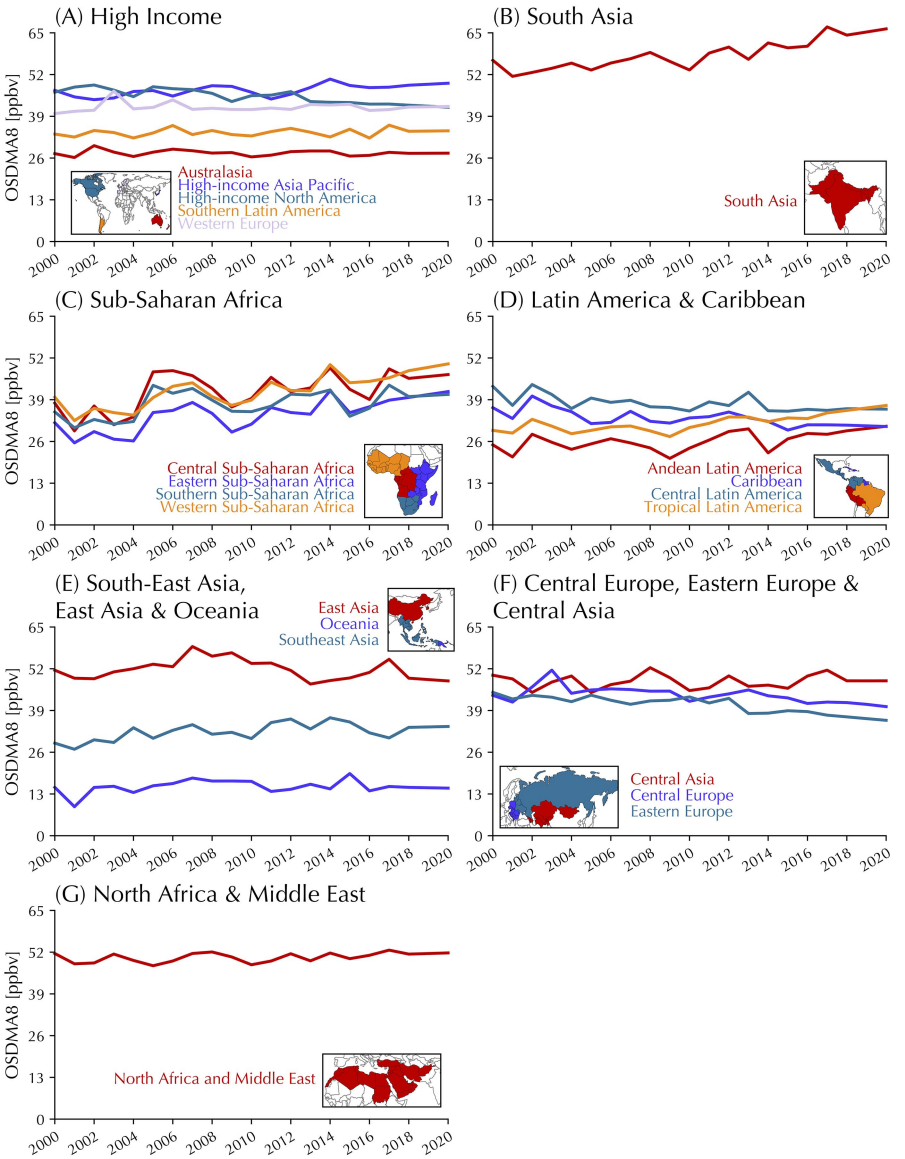


Figure 5. Population-weighted O_3 concentrations estimated using the BME dataset in GBD regions. Each subplot shows population-weighted 2000–2020 OSDMA8 O_3 for regions within each GBD super-region. Shaded countries in each inset map indicate countries that comprise the super-region and are coloured and labelled by the constituent regions.

50 ppbv (figure 5G). In some years, central Sub-Saharan Africa exhibits concentrations similar to those in North Africa and Middle East (e.g. 2005–2006 in figure 5C), while in adjacent years, concentrations can drop nearly 50% (e.g. 2004).

We stress that BME results are estimates that may disagree with other data fusion products or with monitoring networks not used in BME data fusion. For instance, the relatively stable BME OSDMA8 O_3 concentrations in East Asia (figure 5E) differ from the increasing trends reported in East Asia in other studies (e.g. [98–100]). Discrepancies between our BME-derived results and results from observational networks not included in the BME estimation process or other data fusion products may stem from a greater reliance on O_3 simulated with chemical transport models owing to sparse observations or variations in model design and data integration methods [70,101].

Downloaded from royalsocietypublishing.org/rsta/article-pdf/doi/10.1098/rsta.2025.0268/6174166/rsta.2025.0268.pdf
by guest
on 09 November 2026

Accordingly, BME estimates are best interpreted as a spatially complete, internally consistent benchmark for comparison with other products and future trends.

Our long-term trends analysis in figures 3B and 4 covers the last couple of decades, but a contemporaneous global study under the auspices of TOAR-II modelled OSDMA8 O_3 from 1850 to 2014 [102]. OSDMA8 O_3 more than doubled across the northern mid-latitudes since 1850; however, concentrations only showed small increases until around 1950, followed by rapid increases. Concentrations in several high-income regions stabilized by the 1980s and began to decrease in the 2000s, while concentrations in much of the Global South did not experience this stabilization and reduction. Turnock *et al.* [102] also explored drivers of changes in OSDMA8 O_3 from 1850 to 2014. They found that 42% of the changes in global mean OSDMA8 O_3 concentrations over the historical period are due to changes in global NO_x emissions, 14% to changes in global stratospheric O_3, 29% to changes in global CH_4, 7% to changes in global CO and non-CH_4 VOC emissions and 4% from both aerosols and climate change.

7. Ozone-attributable burden of disease

Using the BME dataset to estimate long-term O_3 exposure for a HIA, the GBD Study 2021 identified O_3 as the eighth leading environmental or occupational risk factor for premature death, responsible for an estimated 480 000 COPD deaths (95% CI: 100 000–830 000 deaths) for the population aged 25 and above in 2020 (figure 6A,B). Other HIAs for a similar time period differ in their choice of exposure metrics and datasets, health endpoints (e.g. COPD versus all respiratory mortality, or inclusion of cardiovascular or all-cause mortality) and concentration–response functions. These other studies indicate a different number of attributable deaths but mostly the same order of magnitude (figure 6B). As examples, Malashock *et al.* [76] estimated 423 000 respiratory deaths, and Chen *et al.* [103], who considered both respiratory and circulatory mortality, estimated 970 000 deaths with exposure and population datasets representative of 2019. By contrast, Wang *et al.* [96] applied an all-cause mortality framework and multi-year (2019–2021) average concentrations, resulting in a larger estimated burden of 1.4 million attributable deaths. Recent O_3-attributable premature deaths estimated by the GBD Study 2021 are highest across a broad swath of the northern mid-latitudes, including the United States, southeastern Europe, and Southern and Eastern Asia (figure 6C). At the national level, rates are highest in Nepal and North Korea (18.6 and 16.2 attributable deaths per 100 000, respectively) and lowest for small island nations in Oceania and the Caribbean (fewer than 0.01 deaths per 100 000). These small island nations may not be well resolved in the BME dataset.

Premature mortality attributable to long-term O_3 exposure increased between 2000 and 2020 (figure 6A,B,D). From the GBD Study 2021, estimated deaths increased by 7670 yr^{-1} with very high certainty in this trend. We also see evidence of this growing burden of disease from HIAs complementing the GBD (figure 6B). Although substantial interstudy heterogeneity exists, the mean of reported estimates from studies covering the most recent year, 2019 [76,96,103], is approximately 930 000 attributable deaths yr^{-1} and about 1.9 times higher than the mean estimate for studies centred on 2000 (approx. 500 000 deaths yr^{-1}) [104–106].

Global O_3-attributable mortality rates also increased from 4.91 to 6.13 deaths per 100 000 between 2000 and 2020 (change of 0.06 deaths per 100 000 yr^{-1}, very high certainty), indicating that the growing burden reflects rising per-person risk and not solely population growth and ageing. Trends in O_3-attributable mortality rates are largest in the Global South (figure 6D), a region that has historically faced smaller attributable mortality rates (figure 6C) and fewer cumulative associated deaths (figure 6A), in GBD Study 2021 estimates. Similar to regional trends in O_3 concentrations (§6), 14 of the 21 regions defined by the GBD saw increasing O_3-attributable mortality rates, and trends in all these regions present high or very high certainty (supplementary material, fig. S9). The South Asia and high-income Asia Pacific regions have the steepest increases (0.41 and 0.06 deaths per 100 000 yr^{-1}, respectively; supplementary material, fig. S9). Decreasing trends in

Downloaded from royalsocietypublishing.org/rsta/article-pdf/doi/10.1098/rsta.2025.0268/6174166/rsta.2025.0268.pdf
by guest
on 09 November 2026

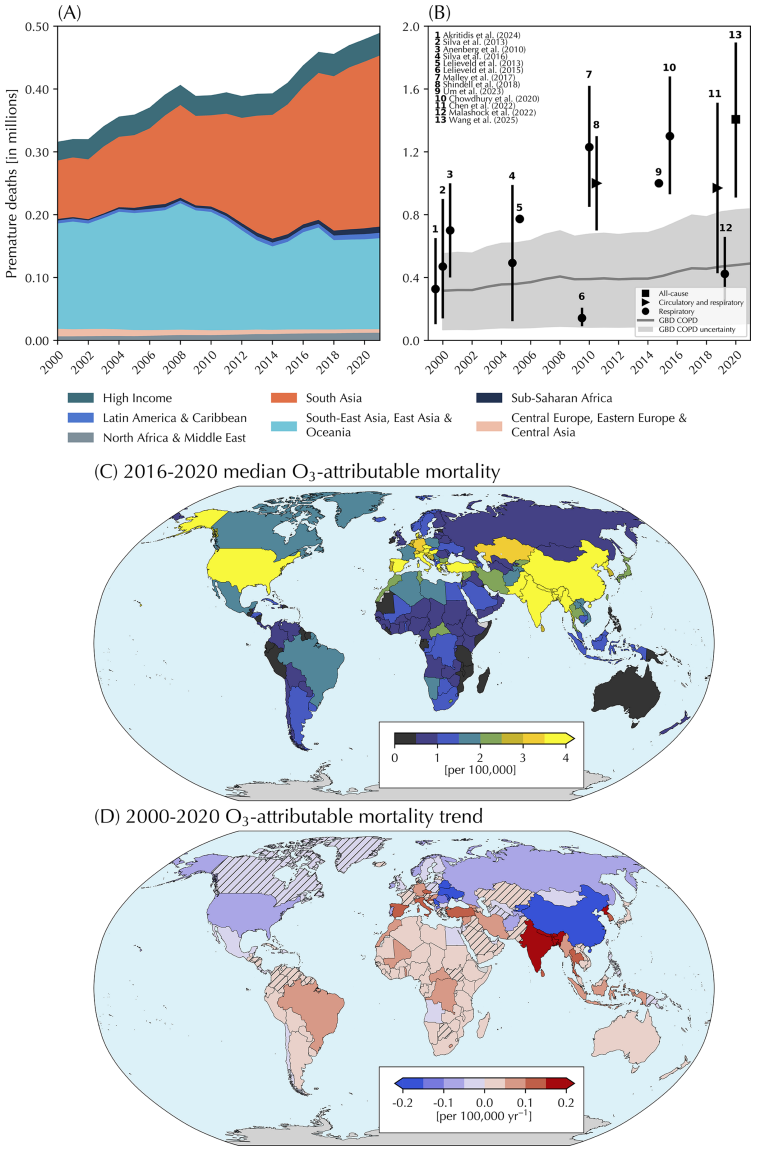


Figure 6. Spatial variations and trends in O_3-attributable premature mortality. (A) The annual number of O_3-attributable premature COPD deaths at the super-region level. (B) Grey time series and shading represent the global (i.e. super-region aggregated) O_3-attributable premature COPD deaths from (A) and the 95% uncertainty interval associated with the global estimates, respectively; scatter points and vertical bars show the central estimate and, when available, associated confidence intervals for global estimates of attributable premature deaths to long-term exposure from the literature. In (B), slight horizontal offsets are applied to studies from the same year to prevent overlapping points (e.g. 1–3). (C) 2016–2020 median national-level premature mortality rates attributable to long-term O_3 exposure. (D) Shading shows 2000–2020 median quantile regression trends in national-level O_3-attributable premature mortality rates, and hatching indicates countries where statistical certainty is medium or lower. Besides values in (B) from the literature, all other data are derived from the GBD Study 2021.

attributable mortality rates were found for seven regions, with five exhibiting very high or high statistical certainty. Rates in the East Asia and Eastern Europe regions show the steepest declines (−0.30 and −0.11 deaths per 100 000 yr^{-1}, respectively).

Individual studies report substantial variability in their central estimates and associated uncertainties (figure 6B). For GBD-sourced estimates, absolute uncertainty increased by a factor of

Downloaded from royalsocietypublishing.org/rsta/article-pdf/doi/10.1098/rsta.2025.0268/6174166/rsta.2025.0268.pdf
by guest
on 09 November 2026

nearly two between 2000 and 2020 (figure 6B), though the coefficient of variation remains approximately constant, indicating relative uncertainty is stable. Across other studies, differences in attributable mortality also reflect methodological choices, including epidemiologic effect estimates, low concentration thresholds and the causes of mortality included. Studies that account for a wider range of impacts, such as child mortality [107,108] or both respiratory and cardiovascular impacts, report more attributable deaths. Even after accounting for these methodological choices, though, differences remain, and Seltzer *et al.* [109] demonstrated that small differences in estimated exposure can be amplified by nonlinear exposure–response curves, underscoring the importance of accurate estimates of O_3 concentrations.

Global and regional increases in premature deaths and mortality rates attributable to long-term exposure raise the question: what is driving these increases since population size, underlying disease rates, and O_3 exposure all changed between 2000 and 2019? Using the BME dataset and decomposition methods to isolate the contribution of each factor to the overall change in attributable mortality, Malashock *et al.* [75] found that increases in O_3 exposure were the dominant driver of rising O_3-attributable deaths between 2000 and 2019 globally, and especially in GBD regions such as southeast Asia, Australasia, Tropical Latin America and regions comprising the Sub-Saharan Africa super-region. Changes in population and population distribution were the second leading factor globally. However, they were the dominant factor in some regions such as North Africa, Middle East and South Asia. Increasing baseline mortality rates in many regions is potentially owing to population ageing and may accentuate the exposure- and population-driven increases in attributable mortality during this period. By contrast, in regions comprising the Sub-Saharan Africa super-region, declining baseline mortality rates offset what could have been even larger increases in attributable deaths owing to increased exposure.

This assessment has emphasized premature mortality from long-term exposure, reflecting both larger epidemiologic effect estimates for long- compared with short-term exposure and the greater severity and valuation weight (e.g. value of a statistical life) of mortality relative to morbidity. However, both long- and short-term exposures have been linked to additional adverse health outcomes (§3). A recent study calculating premature mortality from short-term O_3 exposure estimated 177 000 (95% CI: 139 000, 214 000) deaths globally using 2019–2021 concentrations [96]. Anenberg *et al.* [110] estimated that 9–23 million all-age asthma emergency room visits globally in 2015 were attributable to long-term O_3 exposure.

8. Approaches and uncertainties in ozone health impact assessments

(a) Epidemiologic concentration–response functions

HIAs rely on epidemiologic studies (§3) to provide the concentration–response functions used alongside exposure, population demographics and health data to estimate the disease burden (figure 7). While individual epidemiologic studies focus on specific places, populations and time periods, the concentration–response functions they generate are often applied more broadly in HIAs to different populations, regions, time frames or policy scenarios. In studies included in this assessment, this assumed transferability represents an important, but difficult to quantify, source of uncertainty, particularly outside the contexts represented by the underlying epidemiologic evidence.

(b) Form and inputs to health impacts assessments

Unlike regulatory standards, which emphasize extreme percentiles or exceedances and may not be representative of time-averaged exposure, HIAs rely on continuous exposure distributions to estimate concentration–response relationships across the susceptible population. HIAs typically

Downloaded from royalsocietypublishing.org/rsta/article-pdf/doi/10.1098/rsta.2025.0268/6174166/rsta.2025.0268.pdf
by guest
on 09 November 2026

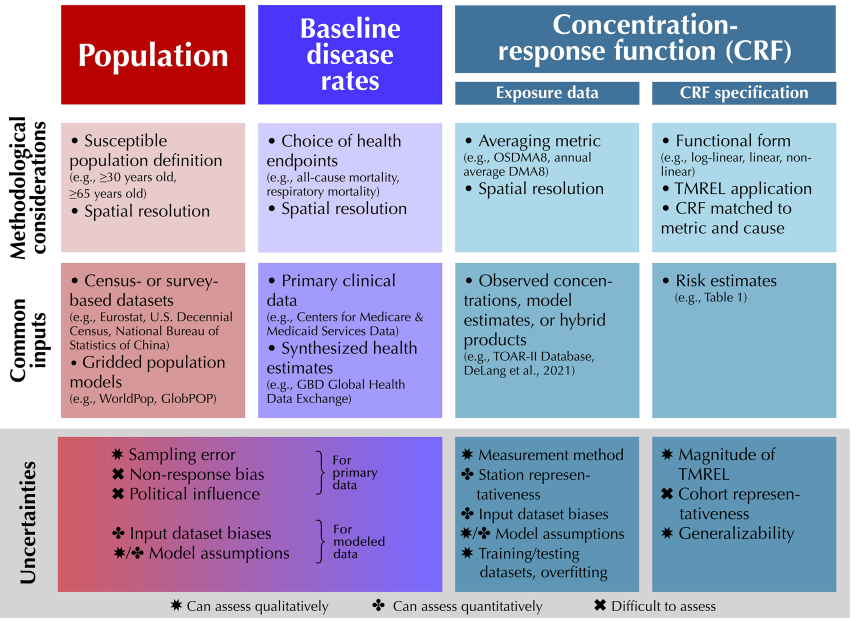


Figure 7. Methodological considerations for and common datasets used in health impact assessments (HIAs) and uncertainties associated with HIAs. Columns in the schematic correspond to different classes of HIA inputs, and boxes that span multiple columns represent aspects that transcend these different classes. Symbols in the 'uncertainties' box correspond to whether and how different types of uncertainty can be quantified and were determined by expert judgement from the TOAR-II Health author team. Acronyms: CRF = concentration–response function, TMREL = theoretical minimum-risk exposure level, GBD = Global Burden of Disease.

estimate O_3-attributable mortality or morbidity as

$$Y = Y_0 \times \text{pop} \times \left[\text{PAF}\left(C_1\right) - \text{PAF}\left(C_0\right)\right], \tag{8.1}$$

where Y is the number of attributable outcomes, Y_0 is the baseline incidence rate, pop is the susceptible population and PAF represents the population attributable fraction—the fraction of the health outcome attributable to exposure—at observed or estimated concentration C_1 and counterfactual concentration C_0. With the commonly used log–linear form, the population attributable fraction is given by

$$\text{PAF}\ (C) = 1 - e^{-\beta C}, \tag{8.2}$$

where β is the coefficient derived from an effect estimate (e.g. hazard ratio, relative risk or odds ratio; see table 1). If $C_1 < C_0$, no attributable outcomes are assumed rather than presented as a benefit. In practice, C in equation (8.2) reflects aggregated health-relevant O_3 metrics rather than raw observations or estimates, and the GBD uses the theoretical minimum risk exposure level (TMREL), the exposure level at which population risk is minimized, to represent C_0. The choice of metric depends on the health outcome: acute endpoints (e.g. daily mortality or hospital admissions) are typically linked to exposure over a few days, while chronic outcomes require annual or seasonal metrics such as annual average DMA8 or OSDMA8. Differencing the PAF at the observed or estimated concentrations and those at the threshold, $\text{PAF}(C_1) - \text{PAF}(C_0)$, rather than at the concentration level, $C_1 - C_0$, ensures that the nonlinear transformation from exposure-related risk to attributable burden in equation (8.2) is preserved.

The calculations in equations (8.1) and (8.2) are typically performed at the level of administrative units (e.g. census tracts, counties) or model grid cells. Here, Y can be calculated for different

Downloaded from royalsocietypublishing.org/rsta/article-pdf/doi/10.1098/rsta.2025.0268/6174166/rsta.2025.0268.pdf
by guest
on 09 November 2026

demographic groups, for example, using age-specific (e.g. [40]) or race-specific (e.g. [41]) effect estimates; incorporating such heterogeneity in particulate matter HIAs has been shown to increase attributable outcomes by better reflecting differences in susceptibility and exposure–response relationships shaped by biological and social factors [111]. Local census, survey and claims-based data available at fine-scale administrative units (e.g. United States Decennial Census, Chinese National Population Census for population data; Medicare and Medicaid for health data) are the most precise options for use in an HIA, although privacy concerns and cost may preclude acquisition and use of these data. In some countries, especially developing or conflict-affected countries, these datasets are only available at a coarse spatial or temporal resolution, or not at all. HIAs increasingly incorporate gridded regional or global estimates of population and population characteristics from products such as WorldPop [112] and estimates of health data that apply small-area estimation approaches or other modelled burden-of-disease frameworks (e.g. GBD DisMOD-MR and WHO life table methodologies) [113,114].

(c) Uncertainty in health impact assessments

Each input in an HIA introduces uncertainty that propagates to the estimates of O_3-attributable mortality or morbidity (figure 7). For instance, observed O_3 concentrations are spatially and temporally limited and may not be representative of actual exposure if monitors are in unique environments (e.g. NO_x titration). Monitors can also be biased by ambient temperature, humidity and cross-species interference [115]. Estimates from statistical or chemical transport models and data fusion products face their own uncertainties: for example, satellite data, which can be incorporated into data fusion products, are subject to a 'clear-sky bias' [116,117], which might lead to apparent underestimates of precursors such as nitrogen dioxide [118]. As true individual-level exposure is not directly observable at a population level, measured or estimated O_3 serves as proxies for true exposure; this limits the quantification of measurement-related uncertainty (figure 7). While geophysical models can estimate O_3 for all-weather conditions, model inputs, parameterization of chemical and physical processes (e.g. vertical mixing, dry deposition), and their resolution can introduce uncertainties and biases [119–122]. Global chemistry transport models face a longstanding challenge: fixed spatial grids introduce numerical diffusion that interacts with sharp dynamical features (frontal systems, filamentary structures), leading to artificially smooth gradients (e.g. [123]) that can introduce biases in monthly averages and obscure true source–receptor relationships (e.g. [124]). When attributing O_3 to different emissions sources or locations, nonlinear chemistry introduces additional uncertainty [125,126]. Statistical and machine learning models can predict O_3 pollution at high resolution with lower computing requirements than geophysical models, but uncertainties arise from training datasets (often geophysical models), risks of overfitting and difficulty of interpretation [74,127]. Quantitative assessment of how biases from spatially unrepresentative training and testing datasets propagate to health impacts remains difficult (figure 7) because the independent, spatially representative observations needed to detect these biases are unavailable where coverage gaps are largest. The duration and definition of the O_3 exposure metric also introduce uncertainty [128,129].

Uncertainty in concentration–response functions stems from errors in measurements or estimates of O_3 exposure, confounder data, sampling error and the assumed function form, which may especially affect the change in risk at lower concentrations [130,131]. Most research linking O_3 exposure with health outcomes has come from North America, Europe and increasingly China [132], raising questions about generalizability. This is especially relevant for O_3 HIAs when target populations are exposed to concentrations outside the range observed in the epidemiologic studies from which concentration–response functions are derived, or when pooling across heterogeneous studies [133]. The inclusion of low-concentration thresholds also introduces uncertainty given the limited number of epidemiologic studies at very low concentrations. Growing evidence indicates that impacts occur even in these ranges [134,135].

Downloaded from royalsocietypublishing.org/rsta/article-pdf/doi/10.1098/rsta.2025.0268/6174166/rsta.2025.0268.pdf
by guest
on 09 November 2026

Population, demographic and health datasets contribute further uncertainty to HIAs. Census- and survey-based datasets are sometimes only available at coarse administrative levels in many countries, and they may suffer from sampling errors [136–138]. Estimated population or demographic data may disagree with each other or with census-based data [139,140], and estimated health data are further complicated by sparse and/or poor-quality records, misclassified diseases or causes of death, incomplete reporting systems and heavy reliance on model output in data-limited settings [141]. In addition, exposure misclassification can arise when population, demographic, health and exposure datasets are aligned but their spatial or temporal resolutions differ.

Across previous studies, uncertainty in O_3 HIAs has been addressed through a range of quantitative approaches that propagate errors from exposure, concentration–response functions, population and health datasets. Traditional statistical methods, including deterministic approaches, have been widely used to quantify sampling error and propagate uncertainty from different HIA inputs [103,142]. Despite its simplicity and utility, deterministic approaches cannot easily account for correlated errors across multiple inputs or provide full probabilistic estimates of combined uncertainty in the final health impact results [143]. Bayesian inference, Monte Carlo simulations and machine learning have all been used to propagate uncertainty in O_3 HIAs, generating probabilistic estimates across inputs and capturing complex distributions. However, each approach requires prior assumptions, computational resources and sufficient data quality [144,145].

9. Future ozone and health

Future changes in O_3-attributable health impacts will be shaped by the combined effects of evolving emissions of precursors; climate change altering the chemical and physical processes that control O_3 formation, removal and transport; and demographic trends that can change population exposure and susceptibility. Quantifying how these factors interact to affect future O_3-attributable mortality has been the focus of many studies, from those isolating the climate-driven impacts within specific climate scenarios—often following representative concentration pathways (RCPs) or shared socioeconomic pathways (SSPs)—to fully combined projections where all drivers evolve together.

The first global estimates of future O_3 health burdens came from studies using combined climate and emission scenarios. West *et al.* [146] estimated global O_3-attributable mortality in 2030 under the Special Report on Emissions Scenarios (SRES) A2 high-emissions scenario (approx. 3.4°C global mean temperature change by the 2090s) and two air quality policy scenario, projecting approximately 500 000 deaths annually under SRES A2 and substantially lower health burdens with stricter emission controls (approx. 190 000 fewer deaths under planned legislation and approx. 460 000 fewer with under maximum feasible reductions). Building on these early scenario-based burden estimates, West *et al.* [147] quantified the global co-benefits of greenhouse gas mitigation by comparing a climate policy scenario (RCP4.5, approx. 2.3°C warming by the 2090s) with a consistent reference case, demonstrating substantial reductions in O_3-attributable mortality in 2030, 2050 and 2100 while accounting for changing population and baseline mortality rates. Selin *et al.* [148] assessed global mortality attributable to O_3 and associated economic impacts by 2050 under the SRES A1B scenario (approx. 2.8°C warming by the 2090s), projecting that O_3-attributable deaths would exceed 2 million annually. Silva *et al.* [149], using a multi-model ensemble from the Atmospheric Chemistry and Climate Model Intercomparison Project (ACCMIP), estimated global O3-attributable mortality rising from 382 000 deaths yr^{-1} in 2000 to 1.09–2.36 million deaths yr^{-1} in 2100 depending on the specific RCP examined. Recent HIAs based on CMIP6 global models, such as Turnock *et al.* [102] and Akritidis *et al.* [106], project that global O_3-attributable excess deaths could reach approximately 2.8–3.5 million yr^{-1} by the end of the century under the high-emissions SSP3-7.0 scenario (approx. 3.6°C warming by the 2090s).

Demographic changes are the dominant driver of projected increases in these global estimates of O_3-attributable mortality, with population growth and ageing contributing the largest shares,

Downloaded from royalsocietypublishing.org/rsta/article-pdf/doi/10.1098/rsta.2025.0268/6174166/rsta.2025.0268.pdf
by guest
on 09 November 2026

while changes in baseline mortality rates, reflecting broader healthcare standards and living conditions, also play a substantial role. Silva *et al.* [149] showed that ageing often outweighs projected exposure changes, with the relative importance varying by specific climate scenarios. Accounting for time-varying baseline mortality rates could lead to an approximately 10% reduction in future O_3-attributable mortality rates under a pessimistic scenario in which CO_2 emissions are projected to roughly double by 2100 relative to current levels (SSP3-7.0) [150]. Akritidis *et al.* [106] further highlighted that under the same scenario (SSP3-7.0), population growth and ageing were responsible for a fivefold increase in global O_3-related mortality at the end of the century, with O_3 increases associated with a factor of 1.6 increase in O_3-attributable mortality. In addition, they suggested that applying the lowest baseline mortality rates observed globally for each age group could reduce the global burden of O_3-attributable mortality by around 30% compared to 2000, even under the high-emissions pathway (SSP3-7.0), highlighting the potential of improved healthcare, nutrition and living conditions to offset environmental risks.

Silva *et al.* [151] estimated that climate change alone could contribute about 44 000 additional O_3-attributable deaths by 2100 under the high-emissions RCP8.5 scenario (approx. 3.7°C warming in the 2090s). More recently, in a single model study, Turnock *et al.* [150] quantified the effect of climate change with two CMIP6 simulations under the SSP3-7.0 emissions scenario, one with varying future sea surface temperatures and one with fixed present-day sea surface temperatures [152] to isolate the influence of climate change via changes in chemistry, emissions, and transport and deposition processes [153]. Differences between these simulations suggested that climate change could increase the global health burden of O_3 by approximately 140 000 deaths yr^{-1} by the end of the century. Applying the same methodology to isolate the climate change effect but using different demographic and health data, Akritidis *et al.* [106] projected that climate change could increase the excess deaths attributable to O_3 by between 42 000 and 217 000 deaths yr^{-1} in 2090. Future climate change may also shape O_3-attributable mortality through additional mechanisms, including synergistic effects of high temperature on O_3-related health risks [154,155] and climate-driven changes in the effectiveness of anthropogenic emission controls [156].

Projected spatial patterns of future O_3-attributable mortality reveal substantial regional disparities with the largest absolute increases of several hundred thousand deaths yr^{-1} in South and East Asia, particularly India and China, owing to large populations, elevated ground-level O_3 concentrations under high-emissions scenarios and high baseline mortality rates [106,150]. In Europe and North America, Silva *et al.* [149] projected decreases in O_3-attributable mortality under most RCPs. Orru *et al.* [157] also projected net reductions in O_3-attributable mortality in Europe by 2050 under an emissions pathway similar to RCP4.5. However, climate change alone would increase O_3 and attributable mortality in southern and central Europe. More recent CMIP6-based analyses suggest increases between 4 and 10 deaths per 100 000 yr^{-1} in O_3-attributable mortality rate under the high-emissions SSP3-7.0 pathway in Western Europe and North America by the end of the century [106,150]. The climate change penalty on surface O_3 under the SSP3-7.0 high-emissions scenario owing to the enhanced efficiency of precursor emissions to produce O_3 [153] is projected to lead to increases in the future health burden of O_3 mainly over East Asia and South Asia [106,150,151,158].

10. Conclusions, recommendations and future directions

Tropospheric O_3 remains a major threat to human health globally, with O_3 exposure and attributable premature mortality changing markedly over the past two decades. The highest recent (2016–2020) O_3 concentrations were observed or estimated in South Asia, the Middle East and parts of East Asia, with generally consistent spatial patterns across exposure metrics (figures 2 and 3). Globally, O_3-attributable mortality nearly doubled from 2000 to 2020 (figures 5 and 6), with a substantial increase in the Global South, reflecting increased exposure and a growing susceptible population. On the other hand, changes in attributable mortality in the Global North slightly declined, reflecting an ageing and more susceptible population offsetting reduced exposure from

Downloaded from royalsocietypublishing.org/rsta/article-pdf/doi/10.1098/rsta.2025.0268/6174166/rsta.2025.0268.pdf
by guest
on 09 November 2026

Table 2. Priority research directions at the O_3-health nexus, reflecting the collective assessment of the TOAR-II Health author team.

domain	priority direction	rationale
observation and estimation	expand surface O_3 monitoring networks in data-sparse regions	new networks in under- or unmonitored regions in Africa, Latin America and Asia enable primary epidemiologic research previously not feasible
	leverage geostationary satellite O_3 retrievals for exposure surveillance	new instruments offer spatially and temporally resolved lower tropospheric estimates in regions lacking monitors
	exploit emerging sensor technology (e.g. low-cost sensors) and methodologies (e.g. ML/AI)	lower instrument cost can enable high-density networks; ML/AI methods can substantially improve raw sensor performance and modelling
	attribute O_3 sources (e.g. stratospheric intrusions, wildfires, long-range transport) relevant to air quality standards	source attribution can distinguish contributions from natural and uncontrollable sources, which are relevant for setting air quality standards, from anthropogenic precursor sectors, where targeted emission reductions remain feasible
exposure metrics and methods	evaluate advanced CRF synthesis methods (e.g. MR-BRT) and co-pollutant adjustment	log–linear O_3 CRFs lag behind $PM_{2.5}$ methodology; co-exposure to NO_2 and $PM_{2.5}$ unresolved
epidemiology	expand epidemiologic evidence to underrepresented regions	O_3 CRFs remain dominated by insights from Europe and North America; Africa, Asia and Latin America are needed to capture full exposure range
	characterize cardiovascular and neurocognitive effects	mechanistic pathways poorly constrained; epidemiologic evidence inconsistent
climate and compound events	quantify compound health impacts of O_3 with heat, $PM_{2.5}$ and wildland fire-sourced $PM_{2.5}$	co-occurring exposures probably amplify burden; future climate will probably shift magnitude and geography of risk

Abbreviations: ML/AI = machine learning/artificial intelligence, CRF = concentration–response function, MR-BRT = Bayesian, regularized, trimmed meta-regression, $PM_{2.5}$ = fine particulate matter with an aerodynamic diameter less than 2.5 µm.

Downloaded from royalsocietypublishing.org/rsta/article-pdf/doi/10.1098/rsta.2025.0268/6174166/rsta.2025.0268.pdf
by guest
on 09 November 2026

regulatory controls on precursor emissions. By linking observationally constrained O_3 exposure fields with GBD-derived health impacts, this assessment shows how spatial patterns and trends in exposure translate into the global distribution of disease burden. While O_3 levels appear to be increasing in many urban environments and across much of the Global South, sparse monitoring coverage in these locales means that differences in levels or trends may fall within the uncertainty of the high-resolution gridded estimates of surface-level O_3 using BME methods (figure 2; supplementary material, figs. S1 and S3).

This assessment underscores the need to substantially expand monitoring coverage—particularly across Africa, South America and Asia, where monitoring coverage remains largely unchanged since *TOAR-I Health*—and data access and availability. A small number of non-quality-controlled observations are available in the TOAR-II database but were excluded from this assessment ('non-profit' monitors; see §4). Some of these are located at United States embassies and consulates in the Global South and provided a rare window into air quality in otherwise under-monitored regions prior to this programme's termination by the United States federal government in 2025 [159]. With appropriate validation and harmonization, such observations should be incorporated into future assessments. Although no universally accepted standard for optimal monitor density exists, guidance from the European Environment Agency (2008) suggests that urban agglomerations of one million people or fewer should be served by at least two monitors, a level of coverage that remains unmet across much of the world. Low-cost sensor networks calibrated through co-location with reference-grade instruments and traceable standards may help expand coverage cost-effectively while maintaining data quality. Expanding monitoring coverage to this or similar levels will require more than ad hoc data collection but rather regional, national and global coordination that enables harmonization, quality control and integration into publicly accessible databases such as TOAR. Clean Air COMPASS (https://cleanaircompass.org), a new open-source air quality data management platform, can further foster collaboration, reduce redundancy and improve data accessibility.

Improving our understanding of O_3-attributable health impacts will require advances spanning observational coverage, improved exposure modelling, and population surveillance and epidemiologic evidence summarized in table 2. Future work should also clearly document which outcomes are included in specific HIAs, as uncertainties in estimates of attributable health impacts are driven primarily by the choice of health outcomes included, exceeding those associated with exposures or individual exposure–response relationships. This uncertainty should be constrained and, when feasible, qualitatively or quantitatively documented (figure 7). Further investigation of how uncertainties in O_3 exposure estimates co-vary with health impact calculations is also needed.

As climate change is expected to increase O_3 exposure in many regions, and shifting population distributions and ageing continue to reshape susceptibility, the global O_3-attributable disease burden will probably grow. Continued reductions in attributable health impacts will depend on maintaining and strengthening existing air quality standards and extending effective emission control strategies to additional regions. Policymakers in regions with increasing O_3 trends might draw on the documented successes in regions with decreasing trends accomplished, in part, by reducing precursor NO_x emissions via vehicle and industrial emissions standards and fuel and technology transitions, while recognizing that climate change and population ageing may necessitate deeper precursor emission reductions to safeguard human health in a changing world.

Ethics. This work did not require ethical approval from a human subject or animal welfare committee.

Data accessibility. All underlying data and code needed to reproduce the analyses and figures are publicly available at [160].

Supplementary material is available online [161].

Declaration of AI use. Artificial intelligence-based tools were used in a limited manner to assist with minor language editing and stylistic refinement. The authors retain full responsibility for the content, analyses and conclusions presented.

Downloaded from royalsocietypublishing.org/rsta/article-pdf/doi/10.1098/rsta.2025.0268/6174166/rsta.2025.0268.pdf
by guest
on 09 November 2026

Authors' contributions. G.H.K.: conceptualization, data curation, formal analysis, investigation, methodology, project administration, resources, software, supervision, validation, visualization, writing—original draft, writing—review and editing; K.A.: conceptualization, data curation, formal analysis, investigation, methodology, writing—original draft, writing—review and editing; L.C.: conceptualization, data curation, formal analysis, investigation, methodology, visualization, writing—original draft, writing—review and editing; J.L.C.: conceptualization, data curation, formal analysis, investigation, methodology, writing—original draft, writing—review and editing; D.S.: conceptualization, data curation, formal analysis, investigation, methodology, writing—original draft, writing—review and editing; D.A.: writing—original draft, writing—review and editing; K.V.: data curation, formal analysis, writing—original draft, writing—review and editing; S.C.A.: writing—original draft, writing—review and editing; C.C.: writing—original draft, writing—review and editing; F.L.: writing—original draft, writing—review and editing; S-Y.K.: writing—original draft, writing—review and editing; J.L.: writing—original draft, writing—review and editing; M.O.N.: writing—original draft, writing—review and editing; P.P.: writing—original draft, writing—review and editing; A.P.: writing—original draft, writing—review and editing; L.R.: writing—original draft, writing—review and editing; E.v.S.: writing—original draft, writing—review and editing; M.G.S.: conceptualization, data curation, writing—original draft, writing—review and editing; S.T.T.: writing—original draft, writing—review and editing; S.W.: writing—original draft, writing—review and editing; J.J.W.: data curation, methodology, validation, writing—original draft, writing—review and editing; Y.Y.: writing—original draft, writing—review and editing.

All authors gave final approval for publication and agreed to be held accountable for the work performed therein.

Conflict of interest declaration. We declare we have no competing interests.

Funding. Research reported in this publication was supported by the National Institute of Environmental Health Sciences of the National Institutes of Health (NIH) through the Research and Engagement for Action on Climate and Health (REACH) Center under award number 1-P20ES036775. The content is solely the responsibility of the authors and does not necessarily represent the official views of the NIH.

Acknowledgements. The authors acknowledge guidance and support from the International Global Atmospheric Chemistry (IGAC) project. TOAR-II has been conducted as a sponsored IGAC Activity. We are grateful to the Helmholtz Association in Germany for funding the TOAR database and web services and to the TOAR database team at Forschungszentrum Jülich for developing and maintaining this infrastructure. Furthermore, we acknowledge all people and agencies that have contributed data to the TOAR database. We also gratefully acknowledge the computing resources provided on the High-Performance Computing Cluster operated by Research Technology Services at the George Washington University [162].

References

1. Fox CB. 1873 *Ozone and antozone: their history and nature. When, where, why, how is ozone observed in the atmosphere?* London: J. & A. Churchill. https://wellcomecollection.org/works/mc74vfhf.
2. Stolarski RS. 2001 History of the study of atmospheric ozone. *Ozone Sci. Eng.* **23**, 421–428. (doi:10.1080/01919510108962025)
3. Haagen-Smit AJ. 1952 Chemistry and physiology of Los Angeles Smog. *Ind. Eng. Chem.* **44**, 1342–1346. (doi:10.1021/ie50510a045)
4. Fowler D *et al.* 2020 A chronology of global air quality. *Phil. Trans. R. Soc. A* **378**, 20 190 314. (doi:10.1098/rsta.2019.0314)
5. Haagen-Smit AJ, Bradley CE, Fox MM. 1953 Ozone formation in photochemical oxidation of organic substances. *Ind. Eng. Chem.* **45**, 2086–2089. (doi:10.1021/ie50525a044)
6. Katz M. 1955 Atmospheric pollution: a growing problem in public health. *Am. J. Public Health* **45**, 298–305. (doi:10.2105/AJPH.45.3.298)
7. Barach AL. 1959 Air pollution and health. *Bull. N. Y. Acad. Med.* **35**, 493–510. (doi:10.1016/b978-012352335-8)
8. Stokinger HE. 1965 Ozone toxicology: a review of research and industrial experience: 1954–1964. *Arch. Environ. Health* **10**, 719–731. (doi:10.1080/00039896.1965.10664082)
9. Joss MK, Eeftens M, Gintowt E, Kappeler R, Künzli N. 2017 Time to harmonize national ambient air quality standards. *Int. J. Public Health* **62**, 453–462. (doi:10.1007/s00038-017-0952-y)
10. Fleming ZL *et al.* 2018 Tropospheric Ozone Assessment Report: present-day ozone distribution and trends relevant to human health. *Elementa* **6**, 12. (doi:10.1525/elementa.273)

Downloaded from royalsocietypublishing.org/rsta/article-pdf/doi/10.1098/rsta.2025.0268/6174166/rsta.2025.0268.pdf
by guest
on 09 November 2026

11. Dentener F (ed.). 2010 *Ozone and particulate matter*. New York, NY: United Nations.
12. Huang M *et al.* 2017 Impact of intercontinental pollution transport on North American ozone air pollution: an HTAP phase 2 multi-model study. *Atmos. Chem. Phys.* **17**, 5721–5750. (doi:10.5194/acp-17-5721-2017)
13. Liang CK *et al.* 2018 HTAP2 multi-model estimates of premature human mortality due to intercontinental transport of air pollution and emission sectors. *Atmos. Chem. Phys.* **18**, 10 497–10 520. (doi:10.5194/acp-18-10497-2018)
14. United Nations Economic Commission for Europe (UNECE). 2023 Addendum—report on the review of the protocol to abate acidification, eutrophication and ground-level ozone, as amended in 2012 [Report of the executive body on its forty-second session]. https://unece.org/environment/documents/2023/03/reports/report-executive-body-its-forty-second-session-addendum.
15. U.S. Environmental Protection Agency. Fact sheet: notice of final rulemaking to reconsider how new source review applies under the phase 1 rule implementing the national air quality standards for 8-hour ozone. https://archive.epa.gov/ttn/ozone/web/pdf/nsr_factsheet.pdf.
16. U.S. Environmental Protection Agency. 1997 National ambient air quality standards for ozone (RIN-2060-AE57). *Fed. Regist.* **62**, 141.
17. World Health Organization. 2021 WHO global air quality guidelines particulate matter (PM2.5 and PM10), ozone, nitrogen dioxide, sulfur dioxide and carbon monoxide. https://www.jstor.org/stable/resrep55512.
18. Mudway I. 2000 Ozone and the lung: a sensitive issue. *Mol. Aspects Med.* **21**, 1–48. (doi:10.1016/S0098-2997(00)00003-0)
19. Nuvolone D, Petri D, Voller F. 2018 The effects of ozone on human health. *Environ. Sci. Pollut. Res.* **25**, 8074–8088. (doi:10.1007/s11356-017-9239-3)
20. Mudway IS, Kelly FJ. 2004 An investigation of inhaled ozone dose and the magnitude of airway inflammation in healthy adults. *Am. J. Respir. Crit. Care Med.* **169**, 1089–1095. (doi:10.1164/rccm.200309-1325PP)
21. Tager IB, Balmes J, Lurmann F, Ngo L, Alcorn S, Künzli N. 2005 Chronic exposure to ambient ozone and lung function in young adults. *Epidemiology* **16**, 751–759. (doi:10.1097/01.ede.0000183166.68809.b0)
22. Brown JS, Bateson TF, McDonnell WF. 2008 Effects of exposure to 0.06 ppm ozone on FEV_1 in humans: a secondary analysis of existing data. *Environ. Health Perspect.* **116**, 1023–1026. (doi:10.1289/ehp.11396)
23. Holm SM, Balmes JR. 2022 Systematic review of ozone effects on human lung function, 2013 through 2020. *Chest* **161**, 190–201. (doi:10.1016/j.chest.2021.07.2170)
24. Abbey DE, Petersen F, Mills PK, Beeson WL. 1993 Long-term ambient concentrations of total suspended particulates, ozone, and sulfur dioxide and Respiratory symptoms in a nonsmoking population. *Arch. Environ. Health* **48**, 33–46. (doi:10.1080/00039896.1993.9938391)
25. Kinney PL, Ware JH, Spengler JD, Dockery DW, Speizer FE, Ferris BG. 1989 Short-term pulmonary function change in association with ozone levels. *Am. Rev. Respir. Dis.* **139**, 56–61. (doi:10.1164/ajrccm/139.1.56)
26. Schwartz J. 1989 Lung function and chronic exposure to air pollution: a cross-sectional analysis of NHANES II. *Environ. Res.* **50**, 309–321. (doi:10.1016/S0013-9351(89)80012-X)
27. U.S. Environmental Protection Agency. 2020 Integrated science assessment for ozone and related photochemical oxidants [*final* report]. https://assessments.epa.gov/isa/document/&deid=348522.
28. Strosnider HM, Chang HH, Darrow LA, Liu Y, Vaidyanathan A, Strickland MJ. 2019 Age-specific associations of ozone and fine particulate matter with respiratory emergency department visits in the United States. *Am. J. Respir. Crit. Care Med.* **199**, 882–890. (doi:10.1164/rccm.201806-1147OC)
29. Ji M, Cohan DS, Bell ML. 2011 Meta-analysis of the association between short-term exposure to ambient ozone and respiratory hospital admissions. *Environ. Res. Lett.* **6**, 024006. (doi:10.1088/1748-9326/6/2/024006)
30. Qiu H, Chuang K-J, Bai C-H, Fan Y-C, Chang T-P, Yim SH-L, Wong T-W, Ho K-F. 2021 Asso-

Downloaded from royalsocietypublishing.org/rsta/article-pdf/doi/10.1098/rsta.2025.0268/6174166/rsta.2025.0268.pdf
by guest
on 09 November 2026

ciation of ambient ozone with pneumonia hospital admissions in Hong Kong and Taipei: a tale of two southeast Asian cities. *Environ. Int.* **156**, 106 634. (doi:10.1016/j.envint.2021.106634)
31. Bell ML. 2004 Ozone and short-term mortality in 95 US urban communities, 1987-2000. *J. Am. Med. Assoc.* **292**, 2372. (doi:10.1001/jama.292.19.2372)
32. Zanobetti A, Schwartz J. 2008 Mortality displacement in the association of ozone with mortality: an analysis of 48 cities in the United States. *Am. J. Respir. Crit. Care Med.* **177**, 184–189. (doi:10.1164/rccm.200706-823OC)
33. Vanos JK, Hebbern C, Cakmak S. 2014 Risk assessment for cardiovascular and respiratory mortality due to air pollution and synoptic meteorology in 10 Canadian cities. *Environ. Pollut.* **185**, 322–332. (doi:10.1016/j.envpol.2013.11.007)
34. Wong CM, Vichit-Vadakan N, Kan H, Qian Z. 2008 Public Health and Air Pollution in Asia (PAPA): a multicity study of short-term effects of air pollution on mortality. *Environ. Health Perspect.* **116**, 1195–1202. (doi:10.1289/ehp.11257)
35. Peng RD *et al.* 2013 Acute effects of ambient ozone on mortality in Europe and North America: results from the APHENA study. *Air Qual. Atmos. Health* **6**, 445–453. (doi:10.1007/s11869-012-0180-9)
36. Vicedo-Cabrera AM *et al.* 2020 Short term association between ozone and mortality: global two stage time series study in 406 locations in 20 countries. *BMJ* **368**, m108. (doi:10.1136/bmj.m108)
37. Martínez-Lazcano JC, González-Guevara E, Del Carmen Rubio M, Franco-Pérez J, Custodio V, Hernández-Cerón M, Livera C, Paz C. 2013 The effects of ozone exposure and associated injury mechanisms on the central nervous system. *Rev. Neurosci.* **24**, 3. (doi:10.1515/revneuro-2012-0084)
38. Devlin RB, Duncan KE, Jardim M, Schmitt MT, Rappold AG, Diaz-Sanchez D. 2012 Controlled exposure of healthy young volunteers to ozone causes cardiovascular effects. *Circulation* **126**, 104–111. (doi:10.1161/CIRCULATIONAHA.112.094359)
39. Jerrett M, Burnett RT, Pope CA, Ito K, Thurston G, Krewski D, Shi Y, Calle E, Thun M. 2009 Long-term ozone exposure and mortality. *N. Engl. J. Med.* **360**, 1085–1095. (doi:10.1056/NEJMoa0803894)
40. Turner MC *et al.* 2016 Long-term ozone exposure and mortality in a large prospective study. *Am. J. Respir. Crit. Care Med.* **193**, 1134–1142. (doi:10.1164/rccm.201508-1633OC)
41. Lim CC, Hayes RB, Ahn J, Shao Y, Silverman DT, Jones RR, Garcia C, Bell ML, Thurston GD. 2019 Long-term exposure to ozone and cause-specific mortality risk in the United States. *Am. J. Respir. Crit. Care Med.* **200**, 1022–1031. (doi:10.1164/rccm.201806-1161OC)
42. Weichenthal S, Pinault LL, Burnett RT. 2017 Impact of oxidant gases on the relationship between outdoor fine particulate air pollution and nonaccidental, cardiovascular, and Respiratory mortality. *Sci. Rep.* **7**, 16 401. (doi:10.1038/s41598-017-16770-y)
43. Niu Y *et al.* 2022 Long-term exposure to ozone and cardiovascular mortality in China: a nationwide cohort study. *Lancet Planet Health* **6**, 496–503. (doi:10.1016/S2542-5196(22)00093-6)
44. Liu S *et al.* 2022 Long-term exposure to ozone and cardiovascular mortality in a large Chinese cohort, Environment International. **165**, 107280 (doi:10.1016/j.envint.2022.107280)
45. Xue T *et al.* 2023 Estimating the exposure–response function between long-term ozone exposure and under-5 mortality in 55 low-income and middle-income countries: a retrospective, multicentre, epidemiological study. *Lancet Planet Health* **7**, 736–746. (doi:10.1016/S2542-5196(23)00165-1)
46. Brauer M *et al.* 2024 Global burden and strength of evidence for 88 risk factors in 204 countries and 811 subnational locations, 1990–2021: a systematic analysis for the Global Burden of Disease Study 2021. *Lancet* **403**, 2162–2203. (doi:10.1016/S0140-6736(24)00933-4)
47. Liu S *et al.* 2022 Long-term exposure to ozone and cardiovascular mortality in a large Chinese cohort. *Environ. Int.* **165**, 107280. (doi:10.1016/j.envint.2022.107280)
48. Delfino RJ, Murphy-Moulton AM, Becklake MR. 1998 Emergency room visits for respiratory illnesses among the elderly in Montreal: association with low level ozone exposure. *Environ. Res.* **76**, 67–77. (doi:10.1006/enrs.1997.3794)
49. Yuan Y, Wang K, Sun HZ, Zhan Y, Yang Z, Hu K, Zhang Y. 2023 Excess mortality associated with high ozone exposure: a national cohort study in China. *Environ. Sci. Ecotechnol.* **15**, 100241. (doi:10.1016/j.ese.2023.100241)

Downloaded from royalsocietypublishing.org/rsta/article-pdf/doi/10.1098/rsta.2025.0268/6174166/rsta.2025.0268.pdf
by guest
on 09 November 2026

50. McConnell R, Berhane K, Gilliland F, London SJ, Islam T, Gauderman WJ, Avol E, Margolis HG, Peters JM. 2002 Asthma in exercising children exposed to ozone: a cohort study. *Lancet* **359**, 386–391. (doi:10.1016/S0140-6736(02)07597-9)
51. McDonnell WF, Abbey DE, Nishino N, Lebowitz MD. 1999 Long-term ambient ozone concentration and the incidence of asthma in nonsmoking adults: the AHSMOG study. *Environ. Res.* **80**, 110–121. (doi:10.1006/enrs.1998.3894)
52. Paulin LM *et al.* 2020 Association of long-term ambient ozone exposure with respiratory morbidity in smokers. *JAMA Intern. Med.* **180**, 106. (doi:10.1001/jamainternmed.2019.5498)
53. Shin S *et al.* 2021 Air pollution as a risk factor for incident chronic obstructive pulmonary disease and asthma. A 15-year population-based cohort study. *Am. J. Respir. Crit. Care Med.* **203**, 1138–1148. (doi:10.1164/rccm.201909-1744OC)
54. Zhao N, Pinault L, Toyib O, Vanos J, Tjepkema M, Cakmak S. 2021 Long-term ozone exposure and mortality from neurological diseases in Canada. *Environ. Int.* **157**, 106 817. (doi:10.1016/j.envint.2021.106817)
55. Gao Q, Zang E, Bi J, Dubrow R, Lowe SR, Chen H, Zeng Y, Shi L, Chen K. 2022 Long-term ozone exposure and cognitive impairment among Chinese older adults: a cohort study. *Environ. Int.* **160**, 107 072. (doi:10.1016/j.envint.2021.107072)
56. Qin MM, Khoshnevis N, Dominici F, Braun D, Zanobetti A, Mork D. 2025 Comparing traditional and causal inference methodologies for evaluating impacts of long-term air pollution exposure on hospitalization with Alzheimer disease and related dementias. *Am. J. Epidemiol.* **194**, 64–72. (doi:10.1093/aje/kwae133)
57. Chen C *et al.* 2022 Association between long-term exposure to ambient air pollution and COVID-19 severity: a prospective cohort study. *CMAJ* **194**, E693–700. (doi:10.1503/cmaj.220068)
58. U.S. Environmental Protection Agency. 2013 Integrated *Science Assessment* (ISA) for ozone and related photochemical oxidants [*final* report]. https://assessments.epa.gov/isa/document/&deid=247492.
59. Cartier JF. 2013 *Canadian smog assessment. Volume 2, health effects*. Ottawa, Canada: Health Canada.
60. Zheng P *et al.* 2022 The burden of proof studies: assessing the evidence of risk. *Nat. Med.* **28**, 2038–2044. (doi:10.1038/s41591-022-01973-2)
61. Raaschou-Nielsen O *et al.* 2013 Air pollution and lung cancer incidence in 17 European cohorts: prospective analyses from the European Study of Cohorts for Air pollution Effects (ESCAPE). *Lancet Oncol.* **14**, 813–822. (doi:10.1016/S1470-2045(13)70279-1)
62. Carey IM, Atkinson RW, Kent AJ, Van Staa T, Cook DG, Anderson HR. 2013 Mortality associations with long-term exposure to outdoor air pollution in a national English cohort. *Am. J. Respir. Crit. Care Med.* **187**, 1226–1233. (doi:10.1164/rccm.201210-1758OC)
63. Strak M *et al.* 2021 Long term exposure to low level air pollution and mortality in eight European cohorts within the ELAPSE project: pooled analysis. *BMJ* **374**, n1904. (doi:10.1136/bmj.n1904)
64. The TOAR Data Team. 2025. *TOAR data progressing [TOAR data technical guide #2]* [Internet]. Jülich: Forschungszentrum Jülich GmbH. https://toar-data.fz-juelich.de/sphinx/TOAR_TG_Vol02_Data_Processing/build/latex/toardataprocessing–technicalguide.pdf.
65. Schultz MG *et al.* 2017 Tropospheric Ozone Assessment Report: database and metrics data of global surface ozone observations. *Elementa* **5**, 58. (doi:10.1525/elementa.244)
66. Chang KL, Schultz MG, Koren G, Selke N. 2025 Guidance note on best statistical practices for TOAR analyses. *arXiv*. (doi:10.48550/arXiv.2304.14236)
67. Galbally IE, Schultz MG, Buchmann B. 2013 *Guidelines for continuous measurements of ozone in the troposphere*. Geneva, Switzerland: World Meteorological Organization.
68. Lefohn AS *et al.* 2018 Tropospheric Ozone Assessment Report: global ozone metrics for climate change, human health, and crop/ecosystem research. *Elem. Sci. Anth.* **6**, 28. (doi:10.1525/elementa.279)
69. DeLang MN *et al.* 2021 Mapping yearly fine resolution global surface ozone through the Bayesian maximum entropy data fusion of observations and model output for 1990–2017. *Environ. Sci. Technol.* **55**, 4389–4398. (doi:10.1021/acs.est.0c07742)

Downloaded from royalsocietypublishing.org/rsta/article-pdf/doi/10.1098/rsta.2025.0268/6174166/rsta.2025.0268.pdf
by guest
on 09 November 2026

70. Wang H *et al.* 2025 Intercomparison of global ground-level ozone datasets for health-relevant metrics. *Atmos. Chem. Phys.* **25**, 15969–15990. (doi:10.5194/egusphere-2024-3723)
71. Wasserstein RL, Schirm AL, Lazar NA. 2019 Moving to a world beyond "$p < 0.05$". *Am. Stat.* **73**, 1–19. (doi:10.1080/00031305.2019.1583913)
72. Mache RK, Schröder S, Langguth M, Patnala A, Schultz MG. 2025 TOAR-classifier v2: a data-driven classification tool for global air quality stations. *EGUsphere*. (doi:10.5194/egusphere-2025-1399)
73. Shi L *et al.* 2021 A national cohort study (2000–2018) of long-term air pollution exposure and incident dementia in older adults in the United States. *Nat. Commun.* **12**, 6754. (doi:10.1038/s41467-021-27049-2)
74. Xue T *et al.* 2020 Estimating spatiotemporal variation in ambient ozone exposure during 2013–2017 using a data-fusion model. *Environ. Sci. Technol.* **54**, 14 877–14 888. (doi:10.1021/acs.est.0c03098)
75. Malashock DA, Delang MN, Becker JS, Serre ML, West JJ, Chang KL, Cooper OR, Anenberg SC. 2022 Global trends in ozone concentration and attributable mortality for urban, peri-urban, and rural areas between 2000 and 2019: a modelling study. *Lancet Planet Health* **6**, e958–67. (doi:10.1016/S2542-5196(22)00260-1)
76. Malashock DA, DeLang MN, Becker JS, Serre ML, West JJ, Chang KL, Cooper OR, Anenberg SC. 2022 Estimates of ozone concentrations and attributable mortality in urban, peri-urban and rural areas worldwide in 2019. *Environ. Res. Lett.* **17**, 054 023. (doi:10.1088/1748-9326/ac66f3)
77. Sun HZ *et al.* 2024 An estimate of global cardiovascular mortality burden attributable to ambient ozone exposure reveals urban-rural environmental injustice. *One Earth* **7**, 1803–1819. (doi:10.1016/j.oneear.2024.08.018)
78. Stevens FR, Gaughan AE, Linard C, Tatem AJ. 2015 Disaggregating census data for population mapping using random forests with remotely-sensed and ancillary data. *PLoS ONE* **10**, e0107042. (doi:10.1371/journal.pone.0107042)
79. Zohdirad H, Montazeri Namin M, Ashrafi K, Aksoyoglu S, Prévôt ASH. 2021 Temporal variations, regional contribution, and cluster analyses of ozone and NOx in a Middle Eastern megacity during summertime over 2017–2019. *Environ. Sci. Pollut. Res.* **29**, 16 233–16 249. (doi:10.1007/s11356-021-14923-1)
80. Khomsi K, Chelhaoui Y, Alilou S, Souri R, Najmi H, Souhaili Z. 2022 Concurrent heat waves and extreme ozone (O_3) episodes: combined atmospheric patterns and impact on human health. *Int. J. Environ. Res. Public Health* **19**, 2770. (doi:10.3390/ijerph19052770)
81. Vohra K, M S, Chakraborty A, Shah H, As. B, Pakki J. 2025 Urgent issues regarding real-time air quality monitoring data in India: unveiling solutions and implications for policy and health. *Atmos. Environ. X* **25**, 100 308. (doi:10.1016/j.aeaoa.2024.100308)
82. Stevenson DS *et al.* 2006 Multimodel ensemble simulations of present-day and near-future tropospheric ozone. *J. Geophys. Res.* **111**, 2005JD006338. (doi:10.1029/2005JD006338)
83. Wild O. 2007 Modelling the global tropospheric ozone budget: exploring the variability in current models. *Atmos. Chem. Phys.* **7**, 2643–2660. (doi:10.5194/acp-7-2643-2007)
84. Goldberg DL, Vinciguerra TP, Hosley KM, Loughner CP, Canty TP, Salawitch RJ, Dickerson RR. 2015 Evidence for an increase in the ozone photochemical lifetime in the eastern United States using a regional air quality model. *JGR Atmos.* **120**, 12 778–12 793. (doi:10.1002/2015JD023930)
85. Prather MJ, Zhu X. 2024 Lifetimes and timescales of tropospheric ozone. *Elem. Sci. Anth.* **12**, 0012. (doi:10.1525/elementa.2023.00112)
86. Becker JS *et al.* 2023 Using regionalized air quality model performance and Bayesian maximum entropy data fusion to map global surface ozone concentration. *Elem. Sci. Anth.* **11**, 00025. (doi:10.1525/elementa.2022.00025)
87. Liu X, Zhu Y, Xue L, Desai AR, Wang H. 2022 Cluster-enhanced ensemble learning for mapping global monthly surface ozone from 2003 to 2019. *Geophys. Res. Lett.* **49**, e2022GL097947. (doi:10.1029/2022GL097947)
88. Gao Z, Wang Y, Vasilakos P, Ivey CE, Do K, Russell AG. 2022 Predicting peak daily maximum 8 h ozone and linkages to emissions and meteorology in southern California using machine learning methods (SoCAB-8HR V1.0). *Geosci. Model Dev.* **15**, 9015–9029. (doi:10.5194/gmd-15-9015-2022)

Downloaded from royalsocietypublishing.org/rsta/article-pdf/doi/10.1098/rsta.2025.0268/6174166/rsta.2025.0268.pdf
by guest
on 09 November 2026

89. Vohra K, Marais EA, Bloss WJ, Schwartz J, Mickley LJ, Van Damme M, Clarisse L, Coheur P-F. 2022 Rapid rise in premature mortality due to anthropogenic air pollution in fast-growing tropical cities from 2005 to 2018. *Sci. Adv.* **8**, eabm4435. (doi:10.1126/sciadv.abm4435)
90. Vazquez Santiago J, Hata H, Martinez-Noriega EJ, Inoue K. 2024 Ozone trends and their sensitivity in global megacities under the warming climate. *Nat. Commun.* **15**, 10 236. (doi:10.1038/s41467-024-54490-w)
91. Gopikrishnan GS, Ardra TS, Kuttippurath J. 2025 Exposure to surface ozone and its associated health effects and economic burden in India. *Glob. Transit.* **7**, 148–158. (doi:10.1016/j.glt.2025.03.002)
92. Rondanelli R, Molina A, Falvey M. 2015 The Atacama surface solar maximum. *Bull. Am. Meteorol. Soc.* **96**, 405–418. (doi:10.1175/BAMS-D-13-00175.1)
93. Galewsky J, Samuels-Crow K. 2014 Water vapor isotopic composition of a stratospheric air intrusion: measurements from the Chajnantor Plateau, Chile. *JGR Atmos.* **119**, 9679–9691. (doi:10.1002/2014JD022047)
94. Pope RJ *et al.* 2020 Substantial increases in eastern Amazon and Cerrado biomass burning-sourced tropospheric ozone. *Geophys. Res. Lett.* **47**, e2019GL084143. (doi:10.1029/2019GL084143)
95. Lee JD *et al.* 2021 Ozone production and precursor emission from wildfires in Africa. *Environ. Sci. Atmos.* **1**, 524–542. (doi:10.1039/D1EA00041A)
96. Wang Y *et al.* 2025 Substantially underestimated global health risks of current ozone pollution. *Nat. Commun.* **16**, 102. (doi:10.1038/s41467-024-55450-0)
97. Zittis G *et al.* 2021 Business-as-usual will lead to super and ultra-extreme heatwaves in the Middle East and North Africa. *npj Clim. Atmos. Sci.* **4**, 20. (doi:10.1038/s41612-021-00178-7)
98. Zhu Q, Bi J, Liu X, Li S, Wang W, Zhao Y, Liu Y. 2022 Satellite-based long-term spatiotemporal patterns of surface ozone concentrations in China: 2005–2019. *Environ. Health Perspect.* **130**, 027 004. (doi:10.1289/EHP9406)
99. Ma D *et al.* 2023 The effect of anthropogenic emission, meteorological factors, and carbon dioxide on the surface ozone increase in China from 2008 to 2018 during the East Asia summer monsoon season. *Atmos. Chem. Phys.* **23**, 6525–6544. (doi:10.5194/acp-23-6525-2023)
100. Li K *et al.* 2025 Surface and tropospheric ozone over East Asia and southeast Asia from observations: distributions, trends, and variability. *EGUsphere*. (doi:10.5194/egusphere-2024-3756)
101. Skipper TN, Hu Y, Odman MT, Henderson BH, Hogrefe C, Mathur R, Russell AG. 2021 Estimating US background ozone using data fusion. *Environ. Sci. Technol.* **55**, 4504–4512. (doi:10.1021/acs.est.0c08625)
102. Turnock S, Akritidis D, Horowitz L, Mertens M, Pozzer A, Reddington C, Wang H, Zhou P, O'Connor F. 2025 Drivers of change in peak season surface ozone concentrations and impacts on human health over the historical period (1850–2014). *Atmos. Chem. Phys.* **25**, 7111–7136. (doi:10.5194/acp-25-7111-2025)
103. Chen L *et al.* 2022 Historical transboundary ozone health impact linked to affluence. *Environ. Res. Lett.* **17**, 104 014. (doi:10.1088/1748-9326/ac9009)
104. Anenberg SC, Horowitz LW, Tong DQ, West JJ. 2010 An estimate of the global burden of anthropogenic ozone and fine particulate matter on premature Human mortality using atmospheric modeling. *Environ. Health Perspect.* **118**, 1189–1195. (doi:10.1289/ehp.0901220)
105. Silva RA *et al.* 2013 Global premature mortality due to anthropogenic outdoor air pollution and the contribution of past climate change. *Environ. Res. Lett.* **8**, 034 005. (doi:10.1088/1748-9326/8/3/034005)
106. Akritidis D *et al.* 2024 Strong increase in mortality attributable to ozone pollution under a climate change and demographic scenario. *Environ. Res. Lett.* **19**, 024 041. (doi:10.1088/1748-9326/ad2162)
107. United Nations Environment Programme, Climate & Clean Air Coalition. 2021 Global methane assessment: benefits and costs of mitigating methane emissions. https://wedocs.unep.org/handle/20.500.11822/35913
108. Shindell D *et al.* 2024 The methane imperative. *Front. Sci.* **2**, 1 349 770. (doi:10.3389/fsci.2024.1349770)
109. Seltzer KM, Shindell DT, Malley CS. 2018 Measurement-based assessment of health burdens from long-term ozone exposure in the United States, Europe, and China. *Environ. Res. Lett.* **13**, 104 018. (doi:10.1088/1748-9326/aae29d)

Downloaded from royalsocietypublishing.org/rsta/article-pdf/doi/10.1098/rsta.2025.0268/6174166/rsta.2025.0268.pdf
by guest
on 09 November 2026

110. Anenberg SC *et al.* 2018 Estimates of the global burden of ambient PM2.5, ozone, and NO_2 on asthma incidence and Emergency room visits. *Environ. Health Perspect.* **126**, 107 004. (doi:10.1289/EHP3766)
111. Spiller E, Proville J, Roy A, Muller NZ. 2021 Mortality risk from PM2.5: a comparison of modeling approaches to identify disparities across racial/ethnic groups in policy outcomes. *Environ. Health Perspect.* **129**, 127 004. (doi:10.1289/EHP9001)
112. Lloyd CT, Sorichetta A, Tatem AJ. 2017 High resolution global gridded data for use in population studies. *Sci. Data* **4**, 170 001. (doi:10.1038/sdata.2017.1)
113. Vos T *et al.* 2017 Global, regional, and national incidence, prevalence, and years lived with disability for 328 diseases and injuries for 195 countries, 1990–2016: a systematic analysis for the Global Burden of Disease Study 2016. *Lancet* **390**, 1211–1259. (doi:10.1016/S0140-6736(17)32154-2)
114. World Health Organization. 2024 WHO methods and data sources for global burden of disease estimates 2000-2021. https://cdn.who.int/media/docs/default-source/gho-documents/global-health-estimates/ghe2021_daly_methods.pdf?sfvrsn=690b16c3_2.
115. Spicer CW, Joseph DW, Ollison WM. 2010 A re-examination of ambient air ozone monitor interferences. *J. Air Waste Manage. Assoc.* **60**, 1353–1364. (doi:10.3155/1047-3289.60.11.1353)
116. Bi J, Belle JH, Wang Y, Lyapustin AI, Wildani A, Liu Y. 2019 Impacts of snow and cloud covers on satellite-derived PM2.5 levels. *Remote Sens. Environ.* **221**, 665–674. (doi:10.1016/j.rse.2018.12.002)
117. Maratt Satheesan S, Eichmann KU, Burrows JP, Weber M, Stauffer R, Thompson AM, Kollonige D. 2024 Improved convective cloud differential (CCD) tropospheric ozone from S5P-TROPOMI satellite data using local cloud fields. *Atmos. Meas. Tech.* **17**, 6459–6484. (doi:10.5194/amt-17-6459-2024)
118. Goldberg DL, Nawaz MO, Lyu C, He J, Carlton AG, Kondragunta S, Anenberg SC. 2025 Clear-sky and cloudy-sky differences in NO_2 concentrations over the United States: implications for satellite measurement applications. *Atmos. Chem. Phys.* **25**, 16 287–16 302. (doi:10.5194/acp-25-16287-2025)
119. Cohan DS, Koo B, Yarwood G. 2010 Influence of uncertain reaction rates on ozone sensitivity to emissions. *Atmos. Environ.* **44**, 3101–3109. (doi:10.1016/j.atmosenv.2010.05.034)
120. Tang W, Cohan DS, Morris GA, Byun DW, Luke WT. 2011 Influence of vertical mixing uncertainties on ozone simulation in CMAQ. *Atmos. Environ.* **45**, 2898–2909. (doi:10.1016/j.atmosenv.2011.01.057)
121. Li D, Liu Z, Zhou M, Zhao Y, Zhang L. 2024 The influence of dry deposition on surface ozone simulations under different planetary boundary layer schemes over eastern China. *Atmos. Environ.* **327**, 120 514. (doi:10.1016/j.atmosenv.2024.120514)
122. Wild O, Prather MJ. 2006 Global tropospheric ozone modeling: quantifying errors due to grid resolution. *J. Geophys Res.* **111**, 2005JD006605. (doi:10.1029/2005JD006605)
123. Rastigejev Y, Park R, Brenner MP, Jacob DJ. 2010 Resolving intercontinental pollution plumes in global models of atmospheric transport. *J. Geophys. Res.* **115**, 2009JD012568. (doi:10.1029/2009JD012568)
124. Yu K *et al.* 2016 Sensitivity to grid resolution in the ability of a chemical transport model to simulate observed oxidant chemistry under high-isoprene conditions. *Atmos. Chem. Phys.* **16**, 4369–4378. (doi:10.5194/acp-16-4369-2016)
125. Ni R, Lin J, Yan Y, Lin W. 2018 Foreign and domestic contributions to springtime ozone over China. *Atmos. Chem. Phys.* **18**, 11 447–11 469. (doi:10.5194/acp-18-11447-2018)
126. Thunis P *et al.* 2019 Source apportionment to support air quality planning: strengths and weaknesses of existing approaches. *Environ. Int.* **130**, 104 825. (doi:10.1016/j.envint.2019.05.019)
127. Pan Q, Harrou F, Sun Y. 2023 A comparison of machine learning methods for ozone pollution prediction. *J. Big Data* **10**, 63. (doi:10.1186/s40537-023-00748-x)
128. Bell ML, Hobbs BF, Ellis H. 2005 Metrics matter: conflicting air quality rankings from different indices of air pollution. *J. Air Waste Manage. Assoc.* **55**, 97–106. (doi:10.1080/10473289.2005.10464596)
129. Digar A, Cohan DS, Bell ML. 2011 Uncertainties influencing health-based prioritization of ozone abatement options. *Environ. Sci. Technol.* **45**, 7761–7767. (doi:10.1021/es200165n)

Downloaded from royalsocietypublishing.org/rsta/article-pdf/doi/10.1098/rsta.2025.0268/6174166/rsta.2025.0268.pdf
by guest
on 09 November 2026

130. Richmond-Bryant J, Mikati I, Benson AF, Luben TJ, Sacks JD. 2020 Disparities in distribution of particulate matter emissions from US coal-fired power plants by race and poverty status after accounting for reductions in operations between 2015 and 2017. *Am. J. Public Health* **110**, 655–661. (doi:10.2105/AJPH.2019.305558)
131. Sheppard L, Burnett RT, Szpiro AA, Kim SY, Jerrett M, Pope CA, Brunekreef B. 2011 Confounding and exposure measurement error in air pollution epidemiology. *Air Qual. Atmos. Health* **5**, 203–216. (doi:10.1007/s11869-011-0140-9)
132. Pozzer A, Anenberg SC, Dey S, Haines A, Lelieveld J, Chowdhury S. 2023 Mortality attributable to ambient air pollution: a review of global estimates. *GeoHealth* **7**, e2022GH000711. (doi:10.1029/2022GH000711)
133. Samet JM. 2008 Air pollution risk estimates: determinants of heterogeneity. *J. Toxicol. Environ. Health Part A* **71**, 578–582. (doi:10.1080/15287390801997666)
134. Crouse DL *et al.* 2015 Ambient $PM_{2.5}$, O_3, and NO_2 exposures and associations with mortality over 16 years of follow-up in the Canadian census Health and Environment cohort (CanCHEC). *Environ. Health Perspect.* **123**, 1180–1186. (doi:10.1289/ehp.1409276)
135. Di Q, Wang Y, Zanobetti A, Wang Y, Koutrakis P, Choirat C, Dominici F, Schwartz JD. 2017 Air pollution and mortality in the Medicare population. *N. Engl. J. Med.* **376**, 2513–2522. (doi:10.1056/NEJMoa1702747)
136. Zablotsky B, Lessem SE, Gindi RM, Maitland AK, Dahlhamer JM, Blumberg SJ. 2023 Overview of the 2019 National Health Interview Survey questionnaire redesign. *Am. J. Public Health* **113**, 408–415. (doi:10.2105/AJPH.2022.307197)
137. Lee S, Brown ER, Grant D, Belin TR, Brick JM. 2009 Exploring nonresponse bias in a health survey using neighborhood characteristics. *Am. J. Public Health.* **99**, 1811–1817. (doi:10.2105/AJPH.2008.154161)
138. Spielman SE, Folch D, Nagle N. 2014 Patterns and causes of uncertainty in the American Community Survey. *Appl. Geogr.* **46**, 147–157. (doi:10.1016/j.apgeog.2013.11.002)
139. Kuffer M, Owusu M, Oliveira L, Sliuzas R, Van Rijn F. 2022 The missing millions in maps: exploring causes of uncertainties in global gridded population datasets. *Int. J. Geoinf.* **11**, 403. (doi:10.3390/ijgi11070403)
140. Chen R, Yan H, Liu F, Du W, Yang Y. 2020 Multiple global population datasets: differences and spatial distribution characteristics. *Int. J. Geoinf.* **9**, 637. (doi:10.3390/ijgi9110637)
141. Naghavi M *et al.* 2024 Global burden of 288 causes of death and life expectancy decomposition in 204 countries and territories and 811 subnational locations, 1990–2021: a systematic analysis for the Global Burden of Disease Study 2021. *Lancet* **403**, 2100–2132. (doi:10.1016/S0140-6736(24)00367-2)
142. Lin J *et al.* 2019 Carbon and health implications of trade restrictions. *Nat. Commun.* **10**, 4947. (doi:10.1038/s41467-019-12890-3)
143. Fornacon-Wood I, Mistry H, Johnson-Hart C, Faivre-Finn C, O'Connor JPB, Price GJ. 2022 Understanding the differences between Bayesian and frequentist statistics. *Int. J. Radiat. Oncol. Biol. Phys.* **112**, 1076–1082. (doi:10.1016/j.ijrobp.2021.12.011)
144. Alexeeff SE, Pfister GG, Nychka D. 2016 A Bayesian model for quantifying the change in mortality associated with future ozone exposures under climate change. *Biometrics* **72**, 281–288. (doi:10.1111/biom.12383)
145. Derwent RG. 2020 Monte Carlo analyses of the uncertainties in the predictions from global tropospheric ozone models: tropospheric burdens and seasonal cycles. *Atmos. Environ.* **231**, 117 545. (doi:10.1016/j.atmosenv.2020.117545)
146. West JJ, Szopa S, Hauglustaine DA. 2007 Human mortality effects of future concentrations of tropospheric ozone. *Comptes Rendus Géosci.* **339**, 775–783. (doi:10.1016/j.crte.2007.08.005)
147. West JJ *et al.* 2013 Co-benefits of mitigating global greenhouse gas emissions for future air quality and human health. *Nat. Clim. Change* **3**, 885–889. (doi:10.1038/nclimate2009)
148. Selin NE, Wu S, Nam KM, Reilly JM, Paltsev S, Prinn RG, Webster MD. 2009 Global health and economic impacts of future ozone pollution. *Environ. Res. Lett.* **4**, 044 014. (doi:10.1088/1748-9326/4/4/044014)
149. Silva RA *et al.* 2016 The effect of future ambient air pollution on human premature mortality to2100 using output from the ACCMIP model ensemble. *Atmos. Chem. Phys.* **16**, 9847–9862. (doi:10.5194/acp-16-9847-2016)

Downloaded from royalsocietypublishing.org/rsta/article-pdf/doi/10.1098/rsta.2025.0268/6174166/rsta.2025.0268.pdf
by guest
on 09 November 2026

150. Turnock ST, Reddington CL, West JJ, O'Connor FM. 2023 The air pollution human health burden in different future scenarios that involve the mitigation of near-term climate forcers, climate and land-use. *GeoHealth* **7**, e2023GH000812. (doi:10.1029/2023GH000812)
151. Silva RA *et al.* 2017 Future global mortality from changes in air pollution attributable to climate change. *Nat. Clim. Change* **7**, 647–651. (doi:10.1038/nclimate3354)
152. Intergovernmental Panel on Climate Change (IPCC). 2023 *Climate change 2021—the physical science basis: Working Group I contribution to the sixth assessment report of the Intergovernmental Panel on Climate Change*, 1st edn. Cambridge: Cambridge University Press. (doi:10.1017/9781009157896)
153. Zanis P *et al.* 2022 Climate change penalty and benefit on surface ozone: a global perspective based on CMIP6 earth system models. *Environ. Res. Lett.* **17**, 024 014. (doi:10.1088/1748-9326/ac4a34)
154. Kahle JJ, Neas LM, Devlin RB, Case MW, Schmitt MT, Madden MC, Diaz-Sanchez D. 2015 Interaction effects of temperature and ozone on lung function and markers of systemic inflammation, coagulation, and fibrinolysis: a crossover study of healthy young volunteers. *Environ. Health Perspect.* **123**, 310–316. (doi:10.1289/ehp.1307986)
155. Wang T *et al.* 2025 Pro-thrombotic changes in response to ambient ozone exposure exacerbated by temperatures. *Environ. Sci. Technol.* **59**, 8391–8401. (doi:10.1021/acs.est.4c13457)
156. Le Roy EJ, Wong AYH, Eastham SD, Fiore AM, Selin NE. 2025 Impact of climate variability and change on the surface ozone response to NO_x emissions reductions. *Environ. Sci. Technol.* **59**, 10 422–10 433. (doi:10.1021/acs.est.5c01347)
157. Orru H, Åström C, Andersson C, Tamm T, Ebi KL, Forsberg B. 2019 Ozone and heat-related mortality in Europe in 2050 significantly affected by changes in climate, population and greenhouse gas emission. *Environ. Res. Lett.* **14**, 074 013. (doi:10.1088/1748-9326/ab1cd9)
158. Im U, Bauer SE, Frohn LM, Geels C, Tsigaridis K, Brandt J. 2023 Present-day and future PM2.5 and O_3-related global and regional premature mortality in the EVAv6.0 health impact assessment model. *Environ. Res.* **216**, 114 702. (doi:10.1016/j.envres.2022.114702)
159. Friedman L, Plumer B. 2025 U.S. State Department shuts down pollution monitoring abroad. *The New York Times*. https://www.nytimes.com/2025/03/04/climate/state-department-air-monitoring-embassies.html.
160. Kerr G *et al.* 2026 Data and code for Tropospheric Ozone Assessment Report II: Changing health impacts of global ozone exposure. [Dataset] In *Phil. Trans. R. Soc. A*. Zenodo. (doi:10.5281/zenodo.21132339)
161. Kerr G *et al.* 2026 Supplementary material from: Tropospheric Ozone Assessment Report II: Changing health impacts of global ozone exposure. Figshare. (doi:10.6084/m9.figshare.c.8654423)
162. MacLachlan G *et al.* 2020 Building a shared resource HPC center across university schools and institutes: a case study. *arXiv*. (doi:10.48550/arXiv.2003.13629)

Downloaded from royalsocietypublishing.org/rsta/article-pdf/doi/10.1098/rsta.2025.0268/6174166/rsta.2025.0268.pdf
by guest
on 09 November 2026